QED theory of scalar hyperfine interactions in HD^+

Tymon Kilich
Faculty of Applied Physics and Mathematics, Gdańsk University of Technology, 80-233 Gdańsk, Poland

Mateusz Pańtak and Krzysztof Pachucki
Faculty of Physics, University of Warsaw, Pasteura 5, 02-093 Warsaw, Poland
(Dated: November 23, 2026)

HD^+ is the simplest heteronuclear molecular ion. It has been used to determine the proton-to-electron and deuteron-to-electron mass ratios, to test quantum electrodynamics, and to search for new interactions. All these applications rely on an accurate knowledge of its hyperfine structure, for which theoretical predictions have disagreed with several precise measurements. Here we calculate the two dominant hyperfine interactions, namely the couplings of the electron spin to the proton and deuteron spins, including the complete nonrecoil electronic relativistic and leading radiative corrections of relative orders α^2 and α^3, respectively, evaluated in the Born-Oppenheimer approximation. Nuclear-structure effects are suppressed by using the measured hyperfine splittings of atomic hydrogen and deuterium. The resulting couplings for 40 rovibrational states are about 18 times more accurate than the previous ones. They agree with the recent Penning-trap measurement in the ground state within the combined uncertainty of 65 Hz, i.e., 7 parts in 10^8, and with a recent measurement in a rotationally excited state, whereas a discrepancy of $7.4(9)$ kHz persists for a vibrational overtone transition. Our results provide improved theoretical input for future determinations of the proton and deuteron masses from HD^+ spectroscopy.

I. INTRODUCTION

The hydrogen molecular ions are the simplest molecules: two nuclei bound by a single electron. Such three-body molecular ions can be both accurately measured [1–9] and accurately calculated from quantum electrodynamics (QED) [10, 11]. For this reason, HD^+ is currently used for the most accurate determination of the proton and deuteron masses in units of the electron mass [12, 13]. HD^+ spectra have also been used in searches for long-range interactions beyond the Standard Model (BSM) [14, 15].

Every rovibrational level of HD^+ is split by the magnetic interactions between the spins of the electron, the proton, and the deuteron, and the rotation of the molecule. This hyperfine structure (hfs) has to be accurately accounted for in order to obtain the spin-averaged transition frequencies from which the mass ratios are determined [13]. In addition, the hyperfine intervals themselves are measured with high accuracy and provide an independent test of the theory. However, significant discrepancies between several measurements and theoretical predictions have been reported for the HD^+ hyperfine splitting [5, 6, 13, 16]. This is surprising, because in another three-body system, namely ^{3}He, theoretical predictions for the hyperfine splitting of the 2^3S_1 state are in very good agreement with the measured values, down to the uncertainty level of 44 Hz. This agreement has been achieved by a complete calculation of the radiative $\alpha\,(Z\,\alpha)^2\,E_F$ correction [17], where E_F is the leading (Fermi) hyperfine energy, α is the fine-structure constant, and Z is the nuclear charge number. We show in this work that the $\alpha\,(Z\,\alpha)^2\,E_F$ correction to the electron–nucleus spin interaction indeed explains the previously reported discrepancies for the hyperfine splitting in the ground $(v, L) = (0, 0)$ [6] and in the rotational $(0, 3)$ [5] levels of HD^+, while the hyperfine splitting in the $(9, 3)$ [1] level remains discrepant.

The hyperfine structure of an arbitrary rovibrational level of HD^+ can be described by an effective Hamiltonian, which consists of all possible couplings between the three spins $\vec{s}_e, \vec{s}_p, \vec{s}_d$ and the angular momentum $\vec{L}$,

$$H_{\rm eff} = A_{ep}\,\vec{s}_e\cdot\vec{s}_p + A_{ed}\,\vec{s}_e\cdot\vec{s}_d + A_{el}\,\vec{s}_e\cdot\vec{L} + A_{pl}\,\vec{s}_p\cdot\vec{L} + A_{dl}\,\vec{s}_d\cdot\vec{L} + A_{pd}\,\vec{s}_p\cdot\vec{s}_d + \dots\,, \quad (1)$$

where $s_e = 1/2$, $s_p = 1/2$, and $s_d = 1$, and the dots denote terms involving four or more powers of spin and angular momentum operators. We concentrate here only on the first two coefficients, A_{ep} and A_{ed} (E_4 and E_5 in Korobov's notation [18]). These two terms are the scalar interactions of the electron spin with the nuclear spins, at the leading order proportional to the electron density at the corresponding nucleus, and are the largest terms in $H_{\rm eff}$. They have, in principle, already been calculated [18–21], but these calculations missed the $(Z\,\alpha)^2\,E_F$ second-order spin–orbit and $\alpha\,(Z\,\alpha)^2\,E_F$ state-dependent corrections.

The calculation of A_{ep} and A_{ed} entirely from first principles would be severely limited by the poorly known nuclear-structure effects. Instead, we rescale the measured hyperfine splittings of atomic hydrogen and deuterium by the ratio of the electron densities at the nucleus in the molecular ion and in the atom. All contributions proportional to this density, including the nuclear-structure ones, are then accounted for by the experimental atomic values, and only the state-dependent contribution is calculated using nonrelativistic quantum electrodynamics (NRQED) and an expansion in α. It is similar to previous calculations by Karr *et al.* [21], where the nuclear-structure correction was extracted from the atomic hyperfine splitting and was then used in HD^+. In our approach, we do not need to consider the contact QED corrections separately, because they are automatically included by rescaling the atomic hyperfine splitting. As a result, only the relativistic $(Z\,\alpha)^2\,E_F$ and radiative $\alpha\,(Z\,\alpha)^2\,E_F$ state-dependent corrections remain to be calculated, while higher-order terms are

neglected, because they are too small to matter at the present level of precision. We derive these two corrections in closed form and evaluate them in the Born–Oppenheimer (BO) approximation, verifying for each of them that the limit of separated atoms reproduces the known hydrogenic result.

The paper is organized as follows. In Sec. II we give an overview of the method and in Sec. III we present the main results and compare them with experiments. The notation and the BO approximation are introduced in Sec. IV, the relativistic and QED corrections to the BO energy in Sec. V, and the expansion of the hyperfine couplings in Sec. VI. The theory of the hfs in hydrogen-like atoms is summarized in Sec. VII. The relativistic correction is derived in Sec. VIII. The final formulas for the radiative correction are presented in Sec. IX, and their derivation in Appendix A. Section X describes the numerical calculations, Sec. XI compares our results with previous calculations, and Sec. XII contains the summary and outlook. Technical details of the numerical calculations and the tabulated potential curves are collected in Appendix B.

II. OVERVIEW OF THE METHOD

Because we aim at an uncertainty much smaller than the nuclear-structure effects, which are difficult to calculate, the scalar couplings for a rovibrational state (v, L) are obtained as

$$A_{e\gamma}(v, L) = \bar{A}_{e\gamma}(v, L) + A^{(6)}_{e\gamma}(v, L) + A^{(7)}_{e\gamma}(v, L) + \dots , \tag{2}$$

a sum of three terms, where $\gamma = p, d$ denotes the nucleus and the dots stand for the neglected higher-order terms. The first term,

$$\bar{A}_{e\gamma}(v, L) = \frac{\langle \pi\, \delta^{(3)}(r_{e\gamma})\rangle_{vL}}{\langle \pi\, \delta^{(3)}(r)\rangle_{\gamma}}\, A^{\rm exp}_{\gamma} , \tag{3}$$

is the measured hyperfine constant $A^{\rm exp}_{\gamma}$ of the hydrogen or deuterium atom, multiplied by the ratio of the electron densities at the nucleus in HD^+ and in the atom. The density in HD^+ is calculated with the full three-body (nonadiabatic) wave function [22]. This term includes the leading Fermi interaction together with those higher-order corrections that are proportional to the electron density at the nucleus, in particular the nuclear-structure effects, which cannot presently be calculated with sufficient accuracy. The second and third terms in Eq. (2) are the remaining corrections of orders $(Z\,\alpha)^2\, E_F$ and $\alpha\,(Z\,\alpha)^2\, E_F$ that are beyond this density scaling. They depend on the molecular state and are the subject of this work. We derive them within NRQED and express them in terms of functions of the internuclear distance R, which are calculated in the BO approximation and then averaged with the nuclear wave function; see Eq. (42) for the exact definition. The complete calculation of these two corrections is the source of the difference from the previous results [21]; see Sec. XI for details. The magnitudes of the individual terms for the ground state are as follows. For the electron–proton coupling, $\bar{A}_{ep} \approx 925$ MHz, $A^{(6)}_{ep} \approx -7.7$ kHz, and $A^{(7)}_{ep} \approx -0.54$ kHz. The uncertainty due to the uncalculated higher-order terms is estimated to be 51 Hz for A_{ep} and 2 Hz for A_{ed}, which is comparable to or smaller than the uncertainty of the most accurate measurement [6].

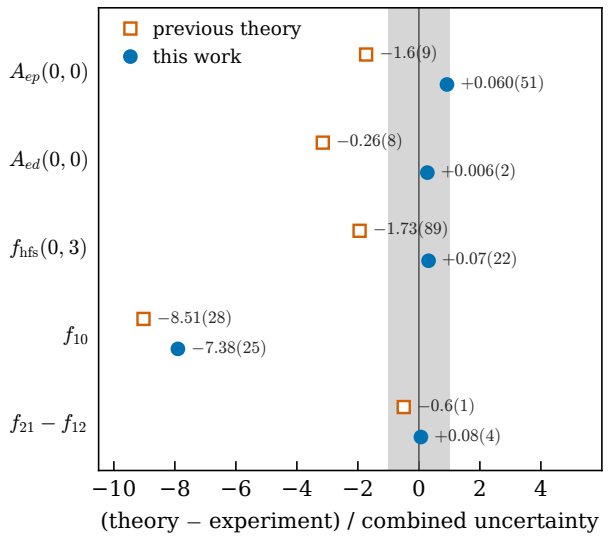

FIG. 1. Deviations of the theoretical predictions from the measured values, divided by the combined theoretical and experimental uncertainty: previous theory (open squares) and this work (full circles). The numbers next to the points are the deviations in kHz, with the theoretical uncertainty in parentheses, and the shaded band is the range of ±1 combined standard deviation. From top to bottom: the scalar couplings A_{ep} and A_{ed} in the ground state $(v, L) = (0, 0)$, Table II; the hyperfine interval $f_{\rm hfs}$ in the $(v, L) = (0, 3)$ state, Table III; the difference f_{10} of two hyperfine components of the $(0, 3) \to (9, 3)$ transition, Table IV; and the difference $f_{21} - f_{12}$ of two hyperfine components of the $(0, 0) \to (5, 1)$ transition, Table V, where the two experimental uncertainties are added in quadrature.

III. RESULTS AND COMPARISON WITH EXPERIMENTS

Our results for the scalar couplings A_{ep} and A_{ed} in the rovibrational states with $0 \le v \le 9$ and $0 \le L \le 3$ are presented in Table I, and their comparison with experiments and with the previous theoretical predictions is summarized in Fig. 1. The uncertainties due to the unknown higher-order terms of Eq. (42) are estimated as follows. The uncertainty due to the Born–Oppenheimer approximation and the neglect of the $(Z\,\alpha)^2\, m/M_\gamma\, E_F$ correction is estimated by $2\, g_\gamma\, m/M_\gamma\, |A^{(6)}_{e\gamma}|$, where the enhancement factor g_γ comes from the second order hyperfine interaction, and a single power of m/M comes from the so-called nonadiabatic perturbation theory [23]. The uncertainty due to the neglect of $A^{(8)}_{e\gamma}$ is estimated by $\alpha\, |A^{(7)}_{e\gamma}|$, because we do not expect any logarithmic enhancements at this order. The final uncertainty is the sum of these two. Analogously, for the difference of the couplings in two states we assume the uncertainty of $2\, g_\gamma\, m/M_\gamma\, |A^{(6)}_{e\gamma}(v, L) - A^{(6)}_{e\gamma}(v', L')| + \alpha\, |A^{(7)}_{e\gamma}(v, L) -$

TABLE I. Electron–proton and electron–deuteron scalar couplings $A_{ep}(v,L)$ and $A_{ed}(v,L)$ (in kHz), from the last columns of Tables X and XI, arranged by the vibrational (v) and rotational (L) quantum numbers. The uncertainties due to the unknown higher-order terms of Eq. (42) are estimated as $2\,g_\gamma\,m/M_\gamma\,|A^{(6)}_{e\gamma}| + \alpha\,|A^{(7)}_{e\gamma}|$, with $A^{(6)}_{e\gamma}$ and $A^{(7)}_{e\gamma}$ from Tables X and XI.

	A_{ep} [kHz]				A_{ed} [kHz]			
v	$L=0$	$L=1$	$L=2$	$L=3$	$L=0$	$L=1$	$L=2$	$L=3$
0	925395.818(51)	924569.375(51)	922925.432(51)	920481.620(51)	142287.827(2)	142160.941(2)	141908.544(2)	141533.344(2)
1	904148.672(49)	903368.031(49)	901815.307(49)	899507.360(49)	139030.350(2)	138910.518(2)	138672.169(2)	138317.893(2)
2	884290.280(47)	883553.314(47)	882087.570(47)	879909.182(47)	135987.377(2)	135874.276(2)	135649.330(2)	135315.022(1)
3	865742.407(45)	865047.215(45)	863664.670(45)	861610.217(45)	133147.139(1)	133040.480(1)	132828.369(1)	132513.178(1)
4	848434.919(43)	847779.812(43)	846477.109(43)	844541.599(43)	130499.186(1)	130398.718(1)	130198.937(1)	129902.117(1)
5	832304.973(41)	831688.462(41)	830462.636(41)	828641.664(41)	128034.294(1)	127939.797(1)	127751.909(1)	127472.809(1)
6	817296.274(39)	816717.053(39)	815565.509(39)	813855.222(39)	125744.392(1)	125655.677(1)	125479.307(1)	125217.373(1)
7	803358.357(37)	802815.294(37)	801735.781(37)	800132.840(37)	123622.516(1)	123539.425(1)	123374.262(1)	123129.031(1)
8	790445.837(35)	789937.960(35)	788928.551(35)	787430.098(35)	121662.795(1)	121585.203(1)	121430.998(1)	121202.105(1)
9	778517.552(33)	778044.037(33)	777103.096(33)	775706.709(33)	119860.481(1)	119788.297(1)	119644.869(1)	119432.050(1)

$A^{(7)}_{e\gamma}(v',L')|$. We should nevertheless mention that estimates of terms that have not yet been calculated are not necessarily reliable. One example is the work of Ref. [21], and another is Ref. [24], where the nonadiabatic effects appear to be 10 times larger than previously estimated [10, 11], although this concerns spin-independent transitions.

In comparison with the previous calculations by Karr *et al.* [21], our results are 18 times more accurate and differ by up to about three of their standard deviations. The source of the difference is the complete (in the BO approximation) calculation of the $(Z\,\alpha)^2\,E_F$ and $\alpha\,(Z\,\alpha)^2\,E_F$ corrections. We have checked the correctness of our results by verifying the large-R asymptotics of $\mathcal{A}^{(7)}_{e\gamma}(R)$, as well as the asymptotics of all other potential curves against the known hydrogenic results.

In Table II we compare our results for the scalar hyperfine interactions in the ground rovibrational state $(v,L)=(0,0)$ with the very recent measurement by König *et al.* [6] and find good agreement, well within the uncertainties.

TABLE II. The scalar spin couplings A_{ep} and A_{ed} of HD^+ in the ground rovibrational state $(v,L)=(0,0)$, in kHz: the recent measurement by König *et al.* [6], with the statistical and systematic uncertainties in the first and second parentheses, this work (Table I), and the previous calculation of Karr *et al.* [21].

	$A_{ep}(0,0)$	$A_{ed}(0,0)$
Experiment [6]	925 395.758(39)(11)	142 287.821(20)(8)
This work	925 395.818(51)	142 287.827(2)
Karr *et al.* [21]	925 394.2(9)	142 287.56(8)

In Table III we compare our result for the hyperfine transition $(F,S,J)=(0,1,4)\to(1,2,5)$ in the $(v,L)=(0,3)$ rovibrational state of HD^+ with the very recent measurement [5] and with previous theoretical predictions from Refs. [5, 16, 20]. Our result is based on the scalar couplings from Table I and the remaining spin–orbit and tensor spin couplings from Refs. [16, 20]; its uncertainty is dominated by the spin–orbit coupling A_{el}. It is in very good agreement with the measured value of Ref. [5].

In Table IV we present our result for the so-called $f_{10}=\nu_{F=0}-\nu_{F=1}$ hyperfine interval, which is the difference between two transition frequencies [1]. Using the notation $(v,L;F,S,J)$ to identify a hyperfine level, the first ($F=0$) transition is $(0,3;0,1,4)\to(9,3;0,1,4)$, and the second ($F=1$) transition is $(0,3;1,2,5)\to(9,3;1,2,5)$. Our calculation of f_{10} is based on A_{ep} and A_{ed} from Table I and the remaining spin–orbit and tensor spin couplings from Refs. [16, 20]. The theoretical uncertainty is again dominated by the electron spin–orbit coupling A_{el}, and we observe a significant discrepancy of 7.4(9) kHz with the measurement [1]. Since we observe very good agreement for the hfs of the $(v,L)=(0,3)$ state in Table III, the discrepancy most likely comes from the $(v,L)=(9,3)$ state, although this comparison alone does not uniquely identify its source. On the theoretical side, all hyperfine coefficients should be verified by nonadiabatic calculations at the $\alpha^2\,E_F$ order. On the experimental side, a hyperfine transition analogous to that of Ref. [5] should be measured within the $(v,L)=(9,3)$ state.

TABLE III. The total hyperfine interval $f_{\rm hfs}$ between the $(F,S,J)=(0,1,4)$ and $(1,2,5)$ levels of HD^+ in the $(v,L)=(0,3)$ state, in kHz. The measurement is from Ref. [5]. Our result is based on the scalar couplings from Table I and all other couplings from Refs. [16, 20]. The previous theoretical predictions are from Ref. [5] and are based on the calculations of Refs. [16, 20].

	$f_{\rm hfs}$
Experiment [5]	1 050 804.511(11)
This work	1 050 804.58(22)
Previous theory [5]	1 050 802.78(89)

TABLE IV. The hyperfine interval f_{10}, which is the difference between two measured $(0,3)\to(9,3)$ transition frequencies in HD^+, in kHz; see the text for details. The measurement is from Ref. [1]. We update the prediction of Ref. [16] with the scalar couplings from Table I.

	f_{10}
Experiment [1]	178 254.4(9)
This work	178 247.02(25)
Haidar *et al.* [16]	178 245.89(28)

In Table V we compare our prediction for the difference $f_{21} - f_{12}$ in the $(v, L) = (0, 0) \to (5, 1)$ transitions with the measurement of Alighanbari *et al.* [4]. The lines f_{12} and f_{21} correspond to the transitions $(G_1, G_2, F) = (1, 2, 2) \to (1, 2, 1)$ and $(0, 1, 1) \to (0, 1, 2)$, respectively (in the notation of Ref. [4], $\vec{G}_1 = \vec{s}_e + \vec{s}_p$, $\vec{G}_2 = \vec{G}_1 + \vec{s}_d$, and $\vec{F} = \vec{G}_2 + \vec{L}$; this is the same coupling scheme as in Ref. [1], only the symbols are different). Our result is based on A_{ep} and A_{ed} from Table I and the remaining couplings from Refs. [4, 16]. It is in slightly better agreement with the measurement than the previous theoretical prediction, but the experimental uncertainty is too large to draw a definite conclusion.

TABLE V. The difference $f_{21} - f_{12}$ of the $(v, L) = (0, 0) \to (5, 1)$ transitions in HD^+, in kHz; see the text for details. The experimental value and the previous theoretical prediction are from Eq. (8) of Ref. [4].

	$f_{21} - f_{12}$
Experiment [4]	126 092.6(1.2)
This work	126 092.68(4)
Previous theory [4]	126 092.0(1)

Although the present calculation resolves the discrepancies in the ground and rotationally excited hyperfine intervals discussed above, some disagreement remains for other rotational transitions, in particular the fundamental rotational transition considered in Ref. [16]. Updating the scalar couplings calculated here does not significantly change this comparison, indicating that further investigation of the remaining hyperfine coefficients is necessary. For instance, the difference $f_{20} - f_{12}$ remains discrepant by approximately 1 kHz, much larger than its experimental uncertainty. Updating the scalar couplings calculated here changes this prediction by only about 20 Hz.

IV. NOTATION AND BORN–OPPENHEIMER APPROXIMATION

To present the calculations, we first introduce the notation. The A coefficients in Eq. (1) are expanded in the fine-structure constant α. In the leading $(Z\,\alpha)^4$ order

$$A^{(4)}_{e\gamma} = \frac{4}{3}\,\frac{Z\,\alpha}{m\,M_\gamma}\,g_\gamma\,\langle\pi\,\delta^{(3)}(r_{e\gamma})\rangle = (Z\,\alpha)^4\,\frac{m^2}{M_\gamma}\,g_\gamma\,\mathcal{A}^{(4)}_{e\gamma}\,, \tag{4}$$

where $\gamma = p, d$, $m \equiv m_e$ is the electron mass, M_γ is the nuclear mass ($M_p \equiv m_p$, $M_d \equiv m_d$), and we have introduced the calligraphic symbol $\mathcal{A}$ to denote a dimensionless quantity. The nuclear "natural" g factor is defined through the nuclear magnetic moment μ,

$$\mu = \frac{Z\,|e|}{2\,M}\,g\,I\,, \tag{5}$$

where I is the nuclear spin, M is the nuclear mass, Z is the nuclear charge in units of the elementary charge, and $e = -|e|$ is the electron charge. The magnetic moments of nuclei are usually given in units of the nuclear magneton $\mu_{\rm N}$,

$$\mu_{\rm N} = \frac{|e|}{2\,m_p}\,. \tag{6}$$

Thus, the nuclear "natural" g factors of the proton and deuteron are

$$g_p = \frac{\mu_p}{\mu_{\rm N}\,I_p}\,, \tag{7}$$

$$g_d = \frac{\mu_d}{\mu_{\rm N}\,I_d}\,\frac{m_d}{m_p}\,, \tag{8}$$

where $I_p = 1/2$ and $I_d = 1$. The relation of the atomic constant A_γ to the ground-state hyperfine splitting is $A_p = \nu_{\rm hfs}({\rm H})$ for hydrogen, and $A_d = \frac{2}{3}\,\nu_{\rm hfs}({\rm D})$ for deuterium. Finally, these hyperfine splittings, magnetic moments, g factors, mass ratios, and fundamental constants used in this work are presented in Table VI.

TABLE VI. Physical constants [12] and experimental hyperfine splittings used in this work [25–27]. Uncertainties in the last digits are given in parentheses.

Quantity	Value	Unit
m_p/m_e	1836.152 673 426(32)	
m_d/m_e	3670.482 967 655(63)	
μ_p	2.792 847 344 63(82)	$\mu_{\rm N}$
μ_d	0.857 438 2335(22)	$\mu_{\rm N}$
g_p	5.585 694 6893(16)	
g_d	1.714 025 4606(44)	
α^{-1}	137.035 999 177(21)	
$R_\infty c$	$3.289\,841\,960\,2500(36) \times 10^{15}$	Hz
$\nu^{\rm exp}_{\rm hfs}({\rm H})$	1 420 405 751.766(3)	Hz
$\nu^{\rm exp}_{\rm hfs}({\rm D})$	327 384 352.522(2)	Hz

We derive formulas and perform calculations in the BO approximation. The total wave function of HD^+ is represented in the BO approximation as

$$\phi_{\rm BO}(\vec{r}_A, \vec{r}_B) = \phi(r_A, r_B, R)\,\frac{\chi_{vL}(R)}{R}\,Y_{LM}\Big(\frac{\vec{R}}{R}\Big)\,, \tag{9}$$

where $R = |\vec{R}_A - \vec{R}_B|$, $r_A = |\vec{r} - \vec{R}_A|$, and $r_B = |\vec{r} - \vec{R}_B|$. The nuclei A and B are the proton and the deuteron, and thus they will also be denoted by $\gamma = p, d$, and the distance between the electron and the nucleus by r_γ. We will use the equivalent notation for the electron–nucleus distance, $r_{e\gamma}$, when full three-body expectation values are considered. The *electronic* wave function ϕ satisfies

$$[\mathcal{H} - \mathcal{E}(R)]|\phi\rangle = 0\,, \tag{10}$$

with the clamped-nuclei Hamiltonian [28]

$$\mathcal{H} = \frac{p^2}{2} - \frac{1}{r_A} - \frac{1}{r_B}\,, \tag{11}$$

where calligraphic symbols denote dimensionless quantities. We define the physical nonrelativistic energy as

$$\mathcal{E}^{(2)}(R) = \mathcal{E}(R) + \frac{1}{R}\,, \tag{12}$$

with the large-R limit

$$\lim_{R\to\infty} \mathcal{E}^{(2)}(R) = -\frac{1}{2}\,. \tag{13}$$

The leading contact hyperfine interaction in Eq. (4) is proportional to

$$D_A(R) = 2\,\pi\,\langle\phi|\delta^{(3)}(r_A)|\phi\rangle\,, \tag{14}$$

with the large-R limit

$$\lim_{R\to\infty} D_A(R) = 1\,, \tag{15}$$

so that $\mathcal{A}^{(4)}_{e\gamma}(R) = \frac{4}{3}\,\langle\pi\,\delta^{(3)}(r_\gamma)\rangle = \frac{2}{3}\,D_\gamma(R)$ in the BO approximation. The radial equation for $\chi_{vL}(R)$ in Eq. (9) is

$$(\mathcal{H}_{\rm BO} - \mathcal{E}_{vL})\,\chi_{vL} = 0\,, \tag{16}$$

where

$$\mathcal{H}_{\rm BO} = -\frac{1}{2\,\mu_{\rm n}}\,\frac{\partial^2}{\partial R^2} + \frac{L\,(L+1)}{2\,\mu_{\rm n}\,R^2} + \tilde{\mathcal{E}}^{(2)}(R)\,, \tag{17}$$

and where

$$\tilde{\mathcal{E}}^{(2)}(R) = \mathcal{E}^{(2)}(R) - \mathcal{E}^{(2)}(\infty)\,, \tag{18}$$

and $\mu_{\rm n}$ is the reduced mass of the proton and deuteron in units of the electron mass,

$$\mu_{\rm n} = \frac{m_p\,m_d}{m\,(m_p+m_d)}\,. \tag{19}$$

Finally, the radial wave function χ_{vL} satisfies the boundary condition $\chi_{vL}(0) = 0$ and the normalization condition

$$\int_0^\infty dR\,\chi^2_{vL}(R) = 1\,. \tag{20}$$

V. RELATIVISTIC AND QED CORRECTIONS TO THE ENERGY

The total BO energy of HD^+ is expanded in powers of α,

$$E(R) = m\,\alpha^2\Big[\mathcal{E}^{(2)}(R) + \alpha^2\,\mathcal{E}^{(4)}(R) + \frac{\alpha^3}{\pi}\,\mathcal{E}^{(5)}(R) + \dots\Big]\,, \tag{21}$$

where $\mathcal{E}^{(2)}(R)$ is defined in Eq. (12), the leading relativistic correction [29] is

$$\mathcal{E}^{(4)}(R) = \langle\mathcal{H}^{(4)}_A\rangle\,, \tag{22}$$

where

$$\mathcal{H}^{(4)}_A = -\frac{p^4}{8} + \frac{\pi}{2}\,[\delta^{(3)}(r_A) + \delta^{(3)}(r_B)]\,. \tag{23}$$

There is also another effective operator, $H^{(4)}_B$, of the same order in $Z\,\alpha$; see Eq. (57). However, its expectation value contributes only to A_{el} in Eq. (1). The large-R asymptotics of $\mathcal{E}^{(4)}$ is

$$\lim_{R\to\infty} \mathcal{E}^{(4)}(R) = -\frac{1}{8}\,. \tag{24}$$

The next term of the α expansion in Eq. (21) is the leading QED correction to the energy [30–32],

$$\mathcal{E}^{(5)}(R) = \left(\frac{4}{3}\,\ln(\alpha^{-2}) + \frac{10}{9} - \frac{4}{15} - \frac{4}{3}\,\ln k_0(R)\right) \times \langle\pi[\delta^{(3)}(r_A) + \delta^{(3)}(r_B)]\rangle\,, \tag{25}$$

where

$$\ln k_0 = \frac{\langle\vec{p}(\mathcal{H}-\mathcal{E})\,\ln[2\,(\mathcal{H}-\mathcal{E})]\,\vec{p}\rangle}{\langle\vec{p}(\mathcal{H}-\mathcal{E})\vec{p}\rangle} = \frac{\langle\vec{p}(\mathcal{H}-\mathcal{E})\,\ln[2\,(\mathcal{H}-\mathcal{E})]\,\vec{p}\rangle}{2\,\pi\,\langle\delta^{(3)}(r_A) + \delta^{(3)}(r_B)\rangle}\,. \tag{26}$$

For the numerical calculation of $\ln k_0$ we use the integral representation

$$\ln k_0 = \frac{1}{D}\int_0^1 dt\,\frac{f(t) - f_0 - f_2\,t^2}{t^3}\,, \tag{27}$$

where

$$D = 2\,\pi\,\langle\delta^{(3)}(r_A) + \delta^{(3)}(r_B)\rangle = D_A + D_B\,, \tag{28}$$

$$f(t) = \left\langle\vec{p}\,\frac{k}{k+\mathcal{H}-\mathcal{E}}\,\vec{p}\right\rangle \text{ with } t = \frac{1}{\sqrt{1+2\,k}}\,. \tag{29}$$

In the numerical calculation it is convenient to use the small-t expansion of $f(t)$ to verify the numerical precision in this difficult region,

$$f(t) = f_0 + f_2\,t^2 + f_3\,t^3 + f_4\,t^4\,\ln(t) + f_5\,t^4 + O(t^5)\,, \tag{30}$$

where

$$f_0 = \langle\vec{p}^{\,2}\rangle\,, \tag{31}$$

$$f_2 = -2\,D\,, \tag{32}$$

$$f_3 = 8\,D\,, \tag{33}$$

$$f_4 = 16\,D\,, \tag{34}$$

$$f_5 = 4\left\langle\left(\frac{\vec{r}_A}{r_A^3} + \frac{\vec{r}_B}{r_B^3}\right)^2\right\rangle + (16\,\ln 2 + 6)\,D\,, \tag{35}$$

where the expectation value $\langle r_\gamma^{-4}\rangle$ is defined in Eq. (77). We verify the numerical calculations against the known large-R asymptotics, which are

$$\lim_{R\to\infty} f_5(R) = 64\,\ln 2 - 20\,, \tag{36}$$

$$\lim_{R\to\infty} \ln k_0(R) = 2.984\,128\,555\,765\,497\,610\,, \tag{37}$$

$$\lim_{R\to\infty} \mathcal{E}^{(5)}(R) = 9.986\,256\,127\,493\,285\,. \tag{38}$$

VI. EXPANSION OF THE HYPERFINE COUPLINGS IN α

We now turn to the hyperfine constants. The coupling $A_{e\gamma}$ can be expanded in powers of α with $Z = 1$,

$$\begin{aligned} A_{e\gamma} &= A^{(4)}_{e\gamma} + A^{(5)}_{e\gamma} + A^{(6)}_{e\gamma} + A^{(7)}_{e\gamma} + \dots \\ &= \alpha^4 \, \frac{m^2}{M_\gamma} \, g_\gamma \left[\mathcal{A}^{(4)}_{e\gamma} + \alpha \, \mathcal{A}^{(5)}_{e\gamma} + \alpha^2 \, \mathcal{A}^{(6)}_{e\gamma} + \frac{\alpha^3}{\pi} \, \mathcal{A}^{(7)}_{e\gamma} \right] . \end{aligned} \tag{39}$$

Because the nuclear-structure contribution is not well known, we calculate $A_{e\gamma}$ as

$$A_{e\gamma} = \frac{\langle \pi \, \delta^{(3)}(r_{e\gamma}) \rangle}{\langle \pi \, \delta^{(3)}(r) \rangle_\gamma} \, A^{\rm exp}_\gamma + \left[A_{e\gamma} - \frac{\langle \pi \, \delta^{(3)}(r_{e\gamma}) \rangle}{\langle \pi \, \delta^{(3)}(r) \rangle_\gamma} \, A_\gamma \right]^{\rm theo} . \tag{40}$$

The first term is the atomic hyperfine splitting scaled by the contact interaction. Namely, the denominator in the first term of Eq. (40) is

$$\langle \pi \, \delta^{(3)}(r) \rangle_\gamma = \left(\frac{m}{M_\gamma} + 1 \right)^{-3} , \tag{41}$$

and the numerator $\langle \pi \, \delta^{(3)}(r_{e\gamma}) \rangle_{vL}$ is the expectation value with the nonadiabatic (full three-body) wave function. The second term, the difference between HD^+ and H (D), is calculated by an expansion in α. The two leading terms in α vanish in this difference, because they are proportional to $\langle \pi \, \delta^{(3)}(r_{e\gamma}) \rangle$. The nonvanishing terms are the state-dependent contributions $A^{(6)}_{e\gamma}$ and $A^{(7)}_{e\gamma}$, and higher-order terms in α are neglected. The $A^{(6)}_{e\gamma}$ and $A^{(7)}_{e\gamma}$ terms are calculated in the BO approximation, so that terms quadratic in the electron-to-nucleus mass ratio are also neglected. The $A_{e\gamma}$ couplings for a given rovibrational state in the BO approximation are obtained from Eq. (40) as

$$\begin{aligned} A_{e\gamma}(v, L) = {} & \frac{\langle \pi \, \delta^{(3)}(r_{e\gamma}) \rangle_{vL}}{\langle \pi \, \delta^{(3)}(r) \rangle_\gamma} \, A^{\rm exp}_\gamma \\ & + \left[\Delta^{(6)}_{vL} + \delta^{(6)}_{vL} \right] (Z \, \alpha)^6 \, \frac{m^2}{M_\gamma} \, g_\gamma \\ & + \left[\Delta^{(7)}_{vL} + \delta^{(7)}_{vL} \right] \frac{\alpha}{\pi} \, (Z \, \alpha)^6 \, \frac{m^2}{M_\gamma} \, g_\gamma \\ \equiv {} & \bar{A}_{e\gamma}(v, L) + A^{(6)}_{e\gamma}(v, L) + A^{(7)}_{e\gamma}(v, L) , \end{aligned} \tag{42}$$

where we keep Z arbitrary only to identify the order of the correction, and

$$\Delta^{(6)}_{vL} = \left\langle v, L \middle| \mathcal{A}^{(6)}_{e\gamma}(R) - \langle \pi \, \delta^{(3)}(r_\gamma) \rangle \, \mathcal{A}^{(6)}_H \middle| v, L \right\rangle , \tag{43}$$

$$\Delta^{(7)}_{vL} = \left\langle v, L \middle| \mathcal{A}^{(7)}_{e\gamma}(R) - \langle \pi \, \delta^{(3)}(r_\gamma) \rangle \, \mathcal{A}^{(7)}_H \middle| v, L \right\rangle , \tag{44}$$

$$\delta^{(6)}_{vL} = 2 \left\langle v, L \middle| \mathcal{E}^{(4)}(R) \, \frac{1}{(\mathcal{E}_{vL} - \mathcal{H}_{\rm BO})'} \, \mathcal{A}^{(4)}_{e\gamma}(R) \middle| v, L \right\rangle , \tag{45}$$

$$\delta^{(7)}_{vL} = 2 \left\langle v, L \middle| \mathcal{E}^{(5)}(R) \, \frac{1}{(\mathcal{E}_{vL} - \mathcal{H}_{\rm BO})'} \, \mathcal{A}^{(4)}_{e\gamma}(R) \middle| v, L \right\rangle + \frac{1}{2} \, \delta^{(6)}_{vL} , \tag{46}$$

where the last term comes from the electron magnetic-moment anomaly, $\langle \pi \, \delta^{(3)}(r_\gamma) \rangle$ is the electronic expectation value at fixed R, and $\mathcal{A}^{(6)}_H$ and $\mathcal{A}^{(7)}_H$ are the corresponding coefficients for the hydrogen atom in the nonrecoil limit.

VII. HYPERFINE SPLITTING IN HYDROGEN-LIKE ATOMS

Let us start the derivation of $\mathcal{A}^{(6)}_{e\gamma}$ and $\mathcal{A}^{(7)}_{e\gamma}$ by summarizing the existing theory of the magnetic-dipole hfs of the $1S$ state of hydrogen-like atoms. To leading order in the fine-structure constant α, it is given by

$$A^{(4)} = E_F = \frac{4}{3} (Z\alpha)^4 \frac{m_{\rm r}^3}{m \, M} \, g , \tag{47}$$

where $m_{\rm r} = mM/(m + M)$ is the reduced mass, m and M are the masses of the electron and the nucleus, respectively, and Z is the nuclear charge number. The leading-order hfs contribution in Eq. (47) is also known as the Fermi energy. The complete hyperfine structure of S states in hydrogenic systems is represented as an expansion in terms of α,

$$A = E_F \, (1 + \delta) , \tag{48}$$

where δ incorporates various corrections. Here we include only the relativistic correction $\delta^{(2)}_H$ and the one-loop radiative correction $\delta^{(3)}_H$, which exhibit a significant state dependence and thus contribute to Δ in Eq. (42),

$$\delta = \kappa + \delta^{(2)}_H + \delta^{(3)}_H . \tag{49}$$

Here, κ is the magnetic-moment anomaly of the free electron, $\kappa = \alpha/(2\pi) + O(\alpha^2)$, and [33]

$$\delta^{(2)}_H = \frac{3}{2} \, (Z \, \alpha)^2 , \tag{50}$$

$$\begin{aligned} \delta^{(3)}_H = {} & \frac{\alpha \, (Z \, \alpha)^2}{\pi} \bigg[- \frac{8}{3} \ln(Z \, \alpha) \Big(\ln(Z \, \alpha) - \ln 4 + \frac{281}{480} \Big) \\ & + 17.122\,338\,751\,3 - \frac{8}{15} \, \ln 2 + \frac{34}{225} \bigg] , \end{aligned} \tag{51}$$

where the first term in the second line comes from the self-energy [34, 35] and the second one from the vacuum polarization. Below we derive the corresponding corrections $A^{(6)}_{e\gamma}$ and $A^{(7)}_{e\gamma}$ for HD^+ and verify that their large-R limits coincide with half of the hydrogen values.

VIII. RELATIVISTIC CORRECTION OF ORDER α^6

The relativistic $\alpha^2 \, E_F$ contribution to the scalar hyperfine couplings is

$$E^{(6)}_{\rm hfs} = \langle H^{(6)}_{\rm hfs} \rangle + 2 \, \langle H^{(4)} \, \frac{1}{(E - H)'} \, H^{(4)}_{\rm hfs} \rangle . \tag{52}$$

The hyperfine Hamiltonian is

$$H_{\rm hfs}^{(4+)} = H_{{\rm hfs},A}^{(4+)} + H_{{\rm hfs},B}^{(4)}\,, \tag{53}$$

$$H_{{\rm hfs},A}^{(4+)} = \frac{2\,Z\,\alpha}{3\,m}\,(1+\kappa)\sum_\gamma \frac{g_\gamma}{M_\gamma}\,\vec{I}_\gamma\cdot\vec{\sigma}\,\pi\,\delta^{(3)}(r_\gamma)\,, \tag{54}$$

$$H_{{\rm hfs},B}^{(4)} = \frac{Z\,\alpha}{2\,m}\sum_\gamma \frac{g_\gamma}{M_\gamma}\,\vec{I}_\gamma\cdot\frac{\vec{r}_\gamma}{r_\gamma^3}\times\vec{p}\,, \tag{55}$$

where $\vec{I}_\gamma \equiv \vec{s}_\gamma$, κ is the electron magnetic-moment anomaly, and $H^{(4+)}$ is the Breit Hamiltonian in the nonrecoil limit,

$$H^{(4+)} = H_A^{(4)} + H_B^{(4+)}\,, \tag{56}$$

$$H_B^{(4+)} = \sum_\gamma \frac{Z\,\alpha}{4\,m^2}\,\frac{\vec{r}_\gamma}{r_\gamma^3}\times\vec{p}\cdot\vec{\sigma}\,(1+2\,\kappa)\,, \tag{57}$$

and $H_A^{(4)}$ is the operator $\mathcal{H}_A^{(4)}$ of Eq. (23) written in natural units.

The operator $H_{\rm hfs}^{(6)}$ in Eq. (52) includes nuclear-spin-dependent operators that contribute at order $m\,\alpha^6$. In hydrogenic systems it leads to $\delta_H^{(2)}$ in Eq. (50). Its derivation for HD^+ proceeds as follows. The vector potential and the magnetic field due to the magnetic moment $\vec{\mu}_\gamma$ of the nucleus γ are

$$e\,\vec{A}_\gamma(\vec{r}) = \frac{e}{4\pi}\,\vec{\mu}_\gamma\times\frac{\vec{r}_\gamma}{r_\gamma^3} = -Z\alpha\,\frac{g_\gamma}{2\,M_\gamma}\vec{I}_\gamma\times\frac{\vec{r}_\gamma}{r_\gamma^3}\,, \tag{58}$$

$$e\,B_\gamma^i(\vec{r}) = e\,(\nabla\times\vec{A}_\gamma)^i = -Z\alpha\,\frac{g_\gamma}{2\,M_\gamma}\frac{8\pi}{3}\delta^{(3)}(r_\gamma)\,I_\gamma^i + Z\alpha\,\frac{g_\gamma}{2\,M_\gamma}\frac{1}{r_\gamma^3}\left(\delta^{ij} - 3\frac{r_\gamma^i r_\gamma^j}{r_\gamma^2}\right)I_\gamma^j\,. \tag{59}$$

Consider the part of the Foldy–Wouthuysen (FW) Hamiltonian [36] that includes the coupling of the electron spin to the magnetic field,

$$\delta H_{\rm FW} = \frac{\vec{\pi}^2}{2\,m} - \frac{e}{2\,m}\,\vec{\sigma}\cdot\vec{B} + \sum_\beta \frac{Z\,\alpha}{4\,m^2}\,\vec{\sigma}\cdot\frac{\vec{r}_\beta}{r_\beta^3}\times\vec{\pi} + \frac{e}{8\,m^3}\left\{\vec{\sigma}\cdot\vec{B}\,,\,\vec{\pi}^2\right\}, \tag{60}$$

where $\vec{\pi} = \vec{p} - e\,\vec{A}$, $\vec{A} = \sum_\gamma \vec{A}_\gamma$, and $\vec{B} = \sum_\gamma \vec{B}_\gamma$. The leading interaction $H_{\rm hfs}^{(4)}$ between the nuclear spins $\vec{I}_\gamma$ and the electron spin $\vec{s}_e = \vec{\sigma}/2$ is obtained from the nonrelativistic terms [the first line of Eq. (60)],

$$H_{\rm hfs}^{(4)} = -\sum_\gamma\left[\frac{e}{m}\,\vec{p}\cdot\vec{A}_\gamma(\vec{r}) + \frac{e}{2\,m}\,\vec{\sigma}\cdot\vec{B}_\gamma(\vec{r})\right], \tag{61}$$

with the vector potential and the magnetic field of the nuclei given by Eqs. (58) and (59). The relativistic correction $H_{\rm hfs}^{(6)}$ is similarly obtained from $\delta H_{\rm FW}$ [the second line of Eq. (60)],

$$H_{\rm hfs}^{(6)} = \sum_\gamma\left[\frac{(Z\,\alpha)^2}{12\,m^2}\,\frac{\vec{r}_\gamma}{r_\gamma^3}\cdot\left(\frac{\vec{r}_A}{r_A^3} + \frac{\vec{r}_B}{r_B^3}\right) - \frac{Z\,\alpha}{6\,m^3}\left\{p^2\,,\,\pi\,\delta^{(3)}(r_\gamma)\right\}\right]\frac{g_\gamma}{M_\gamma}\,\vec{\sigma}\cdot\vec{I}_\gamma\,, \tag{62}$$

in agreement with the earlier, but much lengthier, derivation in Ref. [20]. The total result is

$$A_{e\gamma}^{(6)}(R) = \mathcal{A}_{e\gamma}^{(6)}(R)\,(Z\,\alpha)^6\,\frac{m^2}{M_\gamma}\,g_\gamma\,, \tag{63}$$

$$\mathcal{A}_{e\gamma}^{(6)}(R) = \mathcal{A}_{e\gamma1}^{(6)} + \mathcal{A}_{e\gamma2}^{(6)} + \mathcal{A}_{e\gamma3}^{(6)}\,, \tag{64}$$

$$\mathcal{A}_{e\gamma1}^{(6)} = \left\langle\frac{1}{6}\,\frac{\vec{r}_\gamma}{r_\gamma^3}\cdot\left(\frac{\vec{r}_A}{r_A^3} + \frac{\vec{r}_B}{r_B^3}\right) - \frac{1}{3}\left\{p^2\,,\,\pi\,\delta^{(3)}(r_\gamma)\right\}\right\rangle, \tag{65}$$

$$\mathcal{A}_{e\gamma2}^{(6)} = \frac{2}{3}\left\langle 4\,\pi\,\delta^{(3)}(r_\gamma)\,\frac{1}{(\mathcal{E}-\mathcal{H})'}\times\left(-\frac{p^4}{8} + \frac{\pi}{2}\,[\delta^{(3)}(r_A) + \delta^{(3)}(r_B)]\right)\right\rangle, \tag{66}$$

$$\mathcal{A}_{e\gamma3}^{(6)} = \frac{1}{6}\left\langle\frac{\vec{r}_\gamma}{r_\gamma^3}\times\vec{p}\,\frac{1}{\mathcal{E}-\mathcal{H}}\left(\frac{\vec{r}_A}{r_A^3} + \frac{\vec{r}_B}{r_B^3}\right)\times\vec{p}\right\rangle. \tag{67}$$

However, the above matrix elements are singular. We obtain a finite expression by transforming the operators in the second-order matrix elements according to

$$\mathcal{H}_A^{(4)} \equiv \mathcal{H}_A'^{(4)} + \frac{1}{4}\left\{\frac{1}{r_A} + \frac{1}{r_B}\,,\,\mathcal{E}-\mathcal{H}\right\}, \tag{68}$$

$$4\,\pi\,\delta^{(3)}(r_\gamma) \equiv 4\,\pi\,[\delta^{(3)}(r_\gamma)]' - \left\{\frac{2}{r_\gamma}\,,\,\mathcal{E}-\mathcal{H}\right\}, \tag{69}$$

where the regularized operators are such that

$$4\,\pi\,[\delta^{(3)}(r_\gamma)]'|\phi\rangle = -2\,\frac{\vec{r}_\gamma}{r_\gamma^3}\cdot\vec{\nabla}|\phi\rangle\,, \tag{70}$$

$$\mathcal{H}_A'^{(4)}|\phi\rangle = \left[-\frac{1}{2}\left(\mathcal{E} + \frac{1}{r_A} + \frac{1}{r_B}\right)^2 - \frac{1}{4}\left(\frac{\vec{r}_A}{r_A^3} + \frac{\vec{r}_B}{r_B^3}\right)\cdot\vec{\nabla}\right]|\phi\rangle\,. \tag{71}$$

All singular terms are moved to the first-order matrix elements, which, when combined, form a well-defined and finite expression,

$$\mathcal{A}^{(6)}_{e\gamma} = \frac{1}{3}\left\langle \vec{p}\,\frac{1}{r_\gamma}\left(\mathcal{E}+\frac{1}{r_A}+\frac{1}{r_B}\right)\vec{p}\right\rangle - \frac{2}{3}\left\langle \pi\,\delta^{(3)}(r_\gamma)\right\rangle\left\langle \mathcal{E}+\frac{1}{r_A}+\frac{1}{r_B}\right\rangle + \frac{4}{3}\left\langle\frac{1}{r_\gamma}\right\rangle\mathcal{E}^{(4)} + \frac{2}{3}\left\langle 4\,\pi\,[\delta^{(3)}(r_\gamma)]'\,\frac{1}{(\mathcal{E}-\mathcal{H})'}\,\mathcal{H}'^{(4)}_A\right\rangle + \frac{1}{6}\left\langle\frac{\vec{r}_\gamma}{r^3_\gamma}\times\vec{p}\,\frac{1}{\mathcal{E}-\mathcal{H}}\left(\frac{\vec{r}_A}{r^3_A}+\frac{\vec{r}_B}{r^3_B}\right)\times\vec{p}\right\rangle. \tag{72}$$

Finally, the large-R limit of $\mathcal{A}^{(6)}_{e\gamma}(R)$ is

$$\lim_{R\to\infty}\mathcal{A}^{(6)}_{e\gamma}(R) = \frac{1}{2}\,\mathcal{A}^{(6)}_H = 1\,, \tag{73}$$

which is verified numerically in Table VIII. In the previous calculation of Ref. [20] the last term in Eq. (72) was omitted.

IX. RADIATIVE CORRECTION OF ORDER α^7

The one-loop self-energy and vacuum-polarization corrections to the hfs of order α^7 can be represented as

$$E^{(7)}_{\rm hfs} = E^{(7)}_L + E^{(7)}_{\rm sec} + \langle H^{(7)}_{\rm hfs}\rangle = \sum_\gamma A^{(7)}_{e\gamma}\,\vec{I}_\gamma\cdot\vec{s}_e\,, \tag{74}$$

where $E^{(7)}_L$ is the low-energy contribution with $k\sim m\,\alpha^2$, $E^{(7)}_{\rm sec}$ is the second-order contribution coming from the lower-order effective Hamiltonians $H^{(4)}$ and $H^{(5)}$, and $H^{(7)}_{\rm hfs}$ is a higher-order effective QED Hamiltonian. The derivation of all three parts is presented in Appendix A. They contain the photon-momentum cutoff λ, which cancels out in the sum in Eq. (74). Whenever convenient, we use $A^{(7)}$ or $\mathcal{A}^{(7)}$ instead of $E^{(7)}$. After the elimination of λ and of the divergences, and after matching with the hydrogenic result, $\mathcal{A}^{(7)}_{e\gamma}$ is the sum of three finite terms,

$$\mathcal{A}^{(7)}_{e\gamma} = \mathcal{A}^{(7)}_{L'} + \mathcal{A}^{(7)}_{\rm sec} + \mathcal{A}^{(7)}_{\rm fo}\,, \tag{75}$$

namely the low-energy contribution, the second-order contribution, and the first-order contribution. The first-order contribution includes matrix elements that require a specific definition,

$$\left\langle\frac{1}{r^3_\gamma}\right\rangle = \lim_{\epsilon\to0}\left[\int_{r_\gamma>\epsilon} d^3r\,\frac{\phi^2}{r^3_\gamma} + 4\left\langle\pi\,\delta^{(3)}(r_\gamma)\right\rangle(\gamma_E+\ln\epsilon)\right], \tag{76}$$

$$\left\langle\frac{1}{r^4_\gamma}\right\rangle = \lim_{\epsilon\to0}\left[\int_{r_\gamma>\epsilon} d^3r\,\frac{\phi^2}{r^4_\gamma} - \frac{4\left\langle\pi\,\delta^{(3)}(r_\gamma)\right\rangle}{\epsilon} - 8\left\langle\pi\delta^{(3)}(r_\gamma)\right\rangle(\gamma_E+\ln\epsilon)\right]. \tag{77}$$

Their large-R limits are

$$\lim_{R\to\infty}\left\langle\frac{1}{r^3_\gamma}\right\rangle = \frac{1}{2}\left\langle\frac{1}{r^3}\right\rangle_H = -2\,\ln2\,, \tag{78}$$

$$\lim_{R\to\infty}\left\langle\frac{1}{r^4_\gamma}\right\rangle = \frac{1}{2}\left\langle\frac{1}{r^4}\right\rangle_H = 4\,(\ln2-1)\,. \tag{79}$$

Moreover, for $\phi(\vec{r}) = \phi(r_A, r_B)$ we define $\langle\vec{p}\,\delta^{(3)}(r_A)\,\vec{p}\,\rangle$ as

$$\langle\vec{p}\,\delta^{(3)}(r_A)\,\vec{p}\,\rangle = \left(\frac{\partial\phi}{\partial r_B}\right)^2\Big|_{r_A=0,r_B=R}\,, \tag{80}$$

which vanishes in the hydrogenic and large-R limits. The first-order contribution $\mathcal{A}^{(7)}_{\rm fo}$, after matching with the hydrogenic value, is

$$\mathcal{A}^{(7)}_{\rm fo} = \left\langle\frac{\vec{r}_\gamma}{r^3_\gamma}\cdot\left(\frac{\vec{r}_A}{r^3_A}+\frac{\vec{r}_B}{r^3_B}\right)\right\rangle\left(\frac{4}{9}\,\tau+\frac{7}{24}\right) + \left\langle\frac{1}{r_\gamma}\left(\mathcal{E}^{(2)}+\frac{1}{r_A}+\frac{1}{r_B}-\frac{1}{R}\right)^2\right\rangle\frac{1}{3} + \left\langle\frac{1}{r_\gamma}\right\rangle\mathcal{E}^{(4)}\,\frac{2}{3} + \left\langle\frac{1}{r_A}+\frac{1}{r_B}\right\rangle\left\langle\pi\,\delta^{(3)}(r_\gamma)\right\rangle\left(\frac{32}{9}\,\tau-\frac{1}{3}\right) - \mathcal{E}^{(2)}\left\langle\pi\,\delta^{(3)}(r_\gamma)\right\rangle\left(\frac{16}{9}\,\tau+\frac{5}{18}\right) + \langle\vec{p}\,\pi\,\delta^{(3)}(r_\gamma)\,\vec{p}\,\rangle\left(\frac{8}{9}\,\tau-\frac{1}{36}\right) - \frac{1}{R}\left\langle\pi\delta^{(3)}(r_\gamma)\right\rangle\frac{32}{9}\,\tau + \left\langle\pi\delta^{(3)}(r_\gamma)\right\rangle\left[-\frac{5351}{2700}-\frac{22\pi^2}{27}-\frac{5}{3}\zeta(3)+\frac{448}{27}\ln2+\frac{8}{9}\ln^2 2-\frac{2441}{135}\ln\alpha-\frac{32}{9}\ln^2\alpha+\frac{128}{9}\ln2\ln\alpha\right], \tag{81}$$

where

$$\tau = 5/6 - 1/5 + \ln(\alpha^{-2}/2)\,. \tag{82}$$

The second-order contribution $\mathcal{A}^{(7)}_{\rm sec}$ is

$$\mathcal{A}^{(7)}_{\rm sec} = \frac{2}{9}\,\tau\left\langle 4\,\pi\,[\delta^{(3)}(r_\gamma)]'\,\frac{1}{(\mathcal{E}-\mathcal{H})'}\,4\,\pi\,[\delta^{(3)}(r_A)+\delta^{(3)}(r_B)]'\right\rangle + \frac{1}{3}\left\langle 4\,\pi\,[\delta^{(3)}(r_\gamma)]'\,\frac{1}{(\mathcal{E}-\mathcal{H})'}\,\mathcal{H}'^{(4)}_A\right\rangle + \frac{1}{6}\left\langle \frac{\vec{r}_\gamma}{r_\gamma^3}\times\vec{p}\,\frac{1}{\mathcal{E}-\mathcal{H}}\left(\frac{\vec{r}_A}{r_A^3}+\frac{\vec{r}_B}{r_B^3}\right)\times\vec{p}\right\rangle. \tag{83}$$

The low-energy contribution $\mathcal{A}^{(7)}_{L'}$ of Eq. (A10) is

$$\mathcal{A}^{(7)}_{L'} = \frac{2}{3}\left[\int_0^1 dt\,\frac{f_\gamma(t)-a_\gamma-\sqrt{2}\,b_\gamma\,t+2\,c_\gamma\,\ln(2\,t^2)\,t^2-2\,d_\gamma\,t^2}{t^3}-\sqrt{2}\,b_\gamma-\frac{c_\gamma}{2}\,\ln^2 2+d_\gamma\,\ln 2\right], \tag{84}$$

where the function $f_\gamma(t)$ is defined by Eq. (A3) with $t = 1/\sqrt{1+2\,k}$, and the coefficients a_γ, b_γ, c_γ, and d_γ of its large-k expansion are given in Eqs. (A5)–(A8). Their large-R limits are equal to half of the hydrogenic values [34, 35],

$$\lim_{R\to\infty}\mathcal{A}^{(7)}_{L'}(R) = \frac{2}{3}\left[n_1+n_2+\frac{781}{18}+\frac{4}{3}\,\pi^2-\frac{166}{3}\,\ln 2-\frac{2}{3}\,\ln^2 2\right], \tag{85}$$

$$\lim_{R\to\infty}\mathcal{A}^{(7)}_{\rm sec}(R) = \frac{2}{3}\left[-\frac{125}{36}+\frac{20}{3}\,\ln 2+\frac{40}{3}\,\ln\alpha\right], \tag{86}$$

$$\lim_{R\to\infty}\mathcal{A}^{(7)}_{\rm fo}(R) = \frac{2}{3}\left[-\frac{173}{50}-\frac{11}{18}\,\pi^2+\frac{853}{60}\,\ln 2-2\,\ln^2 2-\frac{2681}{180}\,\ln\alpha+\frac{16}{3}\,\ln 2\,\ln\alpha-\frac{8}{3}\,\ln^2\alpha-\frac{5}{4}\,\zeta(3)\right], \tag{87}$$

$$\lim_{R\to\infty}\mathcal{A}^{(7)}_{e\gamma}(R) = \frac{2}{3}\left[-\frac{8}{3}\ln\alpha\Big(\ln\alpha-2\,\ln 2+\frac{281}{480}\Big)+17.122\,338\,751\,3-\frac{8}{15}\,\ln 2+\frac{34}{225}\right], \tag{88}$$

where n_1 and n_2 are taken from Refs. [34, 35],

$$n_1 = -0.085\,740\,323\,701\,4\,, \tag{89}$$

$$n_2 = 0.067\,496\,936\,500\,3\,. \tag{90}$$

The above asymptotics are verified numerically in Table VIII in Appendix B.

X. NUMERICAL CALCULATIONS

The numerical calculations of $A_{e\gamma}$ are performed according to Eq. (42). The first term, $\bar{A}_{ep}$ ($\bar{A}_{ed}$), is the rescaled atomic hydrogen (deuterium) hyperfine splitting. It involves the electron–nucleus Dirac δ function, whose expectation value with the nonadiabatic wave function is recalculated here using the CODATA 2022 nuclear masses; see Ref. [22] for details and Refs. [37, 38] for the previous calculations. The second and third terms in Eq. (42) are calculated in the BO approximation. Namely, $\mathcal{E}^{(2)}$, $\mathcal{E}^{(4)}$, $\mathcal{E}^{(5)}$, $\mathcal{A}^{(4)}_{e\gamma}$, $\mathcal{A}^{(6)}_{e\gamma}$, and $\mathcal{A}^{(7)}_{e\gamma}$ are calculated on a selected grid of the proton–deuteron distance R, and, in addition, $\mathcal{E}^{(2)}$, $\mathcal{E}^{(4)}$, and $\mathcal{A}^{(4)}_{e\gamma}$ are calculated on the fly for the averaging with the radial function $\chi_{vL}(R)$. Numerically, the most demanding part is the calculation of the Bethe logarithm [39–41] in $\mathcal{E}^{(5)}$ and $\mathcal{A}^{(7)}_{e\gamma}$. We found it numerically efficient to replace the integral over the photon momentum k by an integral over $t = (1+2\,k)^{-1/2}$; see Appendix B for details of the numerical calculations. We have checked analytically and numerically that the large-R asymptotics of $\mathcal{E}^{(5)}$, $\mathcal{A}^{(6)}_{e\gamma}$, and $\mathcal{A}^{(7)}_{e\gamma}$ agree with the hydrogenic values within the quoted numerical precision. Next, we consider the differences

$$\tilde{\mathcal{A}}^{(6)}_{e\gamma}(R) = \mathcal{A}^{(6)}_{e\gamma}(R) - \langle\pi\,\delta^{(3)}(r_\gamma)\rangle\,\mathcal{A}^{(6)}_H\,, \tag{91}$$

$$\tilde{\mathcal{A}}^{(7)}_{e\gamma}(R) = \mathcal{A}^{(7)}_{e\gamma}(R) - \langle\pi\,\delta^{(3)}(r_\gamma)\rangle\,\mathcal{A}^{(7)}_H\,, \tag{92}$$

in which many terms cancel out (see Fig. 2), and calculate their expectation values according to

$$\Delta^{(6)}_{vL} = \big\langle v,L\big|\tilde{\mathcal{A}}^{(6)}_{e\gamma}(R)\big|v,L\big\rangle\,, \tag{93}$$

$$\Delta^{(7)}_{vL} = \big\langle v,L\big|\tilde{\mathcal{A}}^{(7)}_{e\gamma}(R)\big|v,L\big\rangle\,, \tag{94}$$

with radial wave functions obtained using the discrete variable representation (DVR) [42]. Similarly, $\delta^{(6)}_{vL}$ and $\delta^{(7)}_{vL}$ are obtained using a DVR representation of the Hamiltonian $\mathcal{H}_{\rm BO}$, with $\mathcal{E}^{(4)}(R)$ calculated on demand and $\mathcal{E}^{(5)}(R)$ interpolated from the grid values. The numerical results for A_{ep} and A_{ed} are presented in Table I, while the technical details of our numerical calculations and intermediate numerical results are presented in Appendix B. The uncertainties in parentheses account for the unknown higher-order terms of Eq. (42) and are estimated as $2\,g_\gamma\,m/M_\gamma\,|A^{(6)}_{e\gamma}|+\alpha\,|A^{(7)}_{e\gamma}|$, with $A^{(6)}_{e\gamma}$ and $A^{(7)}_{e\gamma}$ from Tables X and XI; they are much larger than our numerical uncertainties. The calculation of these higher-order terms is within reach and would allow one, in the near future, to reduce the uncertainty of the scalar hyperfine couplings in the HD^+ and H_2^+ molecular ions below 10 Hz.

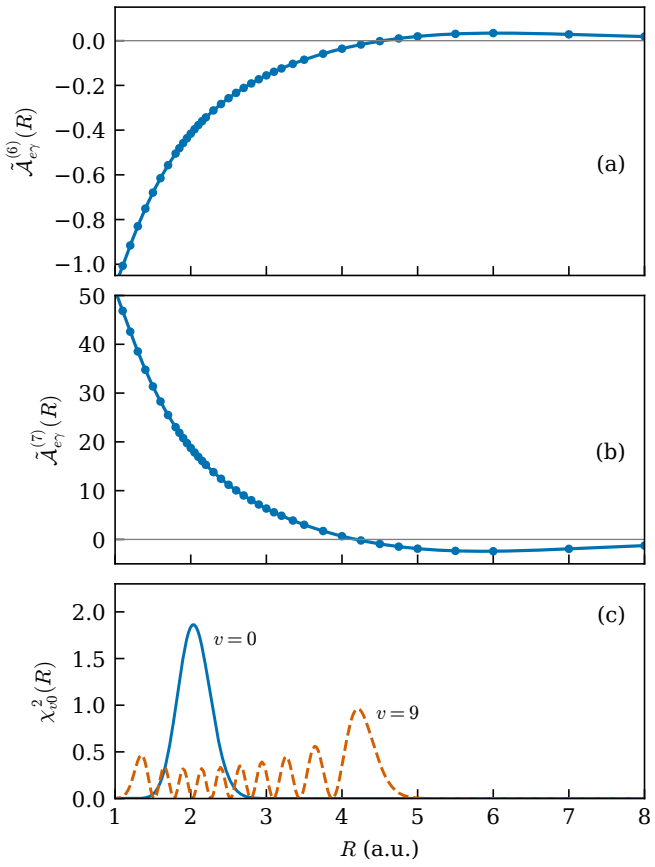

FIG. 2. (a), (b) The functions $\tilde{\mathcal{A}}^{(6)}_{e\gamma}(R)$ and $\tilde{\mathcal{A}}^{(7)}_{e\gamma}(R)$ of Eqs. (91) and (92), i.e., the relativistic and radiative corrections to the scalar coupling with the hydrogenic part subtracted. The points are the calculated values from Table VIII, and the lines are the interpolation used for the rovibrational averaging. Both functions vanish for $R \to \infty$. (c) The probability densities $\chi^2_{vL}(R)$ of the internuclear distance for $L = 0$ and $v = 0$ (solid line) and $v = 9$ (dashed line).

XI. COMPARISON WITH PREVIOUS CALCULATIONS

In Table VII we compare the complete $(Z\,\alpha)^2\,E_F$ correction $\left[\langle\mathcal{A}^{(6)}_{e\gamma}\rangle_{vL} + \delta^{(6)}_{vL}\right](Z\,\alpha)^6\,m^2\,g_\gamma/M_\gamma$ for the relevant rovibrational states $(v, L) = (0, 0)$, $(0, 3)$, and $(9, 3)$, with that of Karr *et al.* [21]. They included the rovibrational contribution $\delta^{(6)}_{vL}$ of Eq. (45), but neglected the second-order spin–orbit term $\mathcal{A}^{(6)}_{e\gamma 3}$ of Eq. (67). As shown in Table VII, omitting this term brings our results into agreement with Ref. [21] to about 0.05 kHz for A_{ep} and 0.007 kHz for A_{ed}, comparable to their numerical precision and also to the uncertainty due to the BO approximation in our calculations.

The total difference from the previous results of Ref. [21] originates from the complete calculation of the relativistic and radiative corrections, in particular from the inclusion of the second-order spin–orbit contribution and the full state-dependent radiative correction $\tilde{\mathcal{A}}^{(7)}_{e\gamma}$.

TABLE VII. Relativistic $(Z\,\alpha)^2 E_F$ contributions to the HD^+ scalar couplings in kHz. The results of Ref. [21] are compared with our calculations without (w/o) and with the second-order spin–orbit contribution $\mathcal{A}^{(6)}_{e\gamma 3}$ of Eq. (67); the latter is our complete result without subtraction of the hydrogenic term $\mathcal{A}^{(6)}_H$.

	$A^{(6)}_{ep}$			$A^{(6)}_{ed}$		
(v, L)	Ref. [21]	w/o	with	Ref. [21]	w/o	with
$(0, 0)$	66.9	66.950	66.300	10.27	10.277	10.177
$(0, 3)$	66.5	66.466	65.825	10.20	10.203	10.105
$(9, 3)$	57.2	57.243	56.897	8.79	8.787	8.734

XII. SUMMARY AND OUTLOOK

We have calculated the scalar spin interactions $A_{ep}\,\vec{s}_e \cdot \vec{s}_p$ and $A_{ed}\,\vec{s}_e \cdot \vec{s}_d$ in the HD^+ molecular ion using the NRQED approach and the experimental values of the hydrogen and deuterium hyperfine splittings, according to Eq. (40). We rescaled the measured atomic hfs by the ratio of the electron densities at the nucleus and calculated the state-dependent remainder in the BO approximation. More precisely, we have obtained closed formulas for $A^{(6)}_{e\gamma}$ and $A^{(7)}_{e\gamma}$ and calculated them numerically in the clamped-nuclei approximation on a large grid of internuclear distances. Next, we used the DVR method to calculate $A_{e\gamma}$ for the rovibrational states with $0 \le v \le 9$ and $0 \le L \le 3$.

Our numerical results in Table I are 18 times more accurate than the previous results of Karr *et al.* [21] and differ by up to about three of their standard deviations. Moreover, our calculations are in agreement with the measurements of the hyperfine splittings in the $(v, L) = (0, 0)$ [6] and $(v, L) = (0, 3)$ [5] states, but disagree with the measurement [1] for the $(v, L) = (0, 3) \to (9, 3)$ transition. Since the hyperfine structure of the $(0, 3)$ state is now confirmed experimentally, the remaining discrepancy of $7.4(9)$ kHz may originate from an unaccounted contribution to the hyperfine structure of the $(9, 3)$ state or from an experimental systematic effect in the overtone measurement. Its explanation requires an independent measurement of a hyperfine interval within this state and a verification of the spin–orbit and tensor couplings, which dominate the present theoretical uncertainty.

The new results for $A_{e\gamma}$ provide improved input for extracting spin-averaged frequencies and determining mass ratios from measurements of transition frequencies between rovibrational states of HD^+ [1, 3, 4]. Moreover, Table VIII provides the data needed to calculate the scalar hyperfine couplings in all other isotopologues; these have to be supplemented by the nuclear g factors and masses and by the finite-mass (nonadiabatic) contact densities.

The theoretical accuracy of A_{ep} and A_{ed} can be improved down to 10 Hz by a nonadiabatic calculation of the $(Z\,\alpha)^2\,E_F$ and $(m/M)\,(Z\,\alpha)^2\,E_F$ corrections, which would allow for more accurate tests of bound-state QED and a more sensitive search for spin-dependent long-range BSM interactions. Moreover, a weighted difference similar to Eq. (40) can be formed for spin-averaged transitions using the extremely ac-

curate measurements of the $1S$–$2S$ transition in H and D. This would enable a more accurate comparison of theoretical predictions with measured transitions in H_2^+ and HD^+, and consequently a significantly more accurate determination of the proton and deuteron masses.

DATA AVAILABILITY

All data that support the findings of this article are included in the article, in particular in Tables I and VIII–XI.

USE OF AI TOOLS

The numerical calculations described in Appendix B, including the codes, the figures, and parts of the text of Appendix B, were prepared with the assistance of the AI system Claude (Anthropic). The authors have reviewed the content and take full responsibility for it.

[1] S. Patra, M. Germann, J.-Ph. Karr, M. Haidar, L. Hilico, V. I. Korobov, F. M. J. Cozijn, K. S. E. Eikema, W. Ubachs, and J. C. J. Koelemeij, Proton-electron mass ratio from laser spectroscopy of HD^+ at the part-per-trillion level, Science **369**, 1238 (2020).

[2] S. Alighanbari, G. S. Giri, F. L. Constantin, V. I. Korobov, and S. Schiller, Precise test of quantum electrodynamics and determination of fundamental constants with HD^+ ions, Nature (London) **581**, 152 (2020).

[3] I. V. Kortunov, S. Alighanbari, M. G. Hansen, G. S. Giri, V. I. Korobov, and S. Schiller, Proton–electron mass ratio by high-resolution optical spectroscopy of ion ensembles in the resolved-carrier regime, Nat. Phys. **17**, 569 (2021).

[4] S. Alighanbari, I. V. Kortunov, G. S. Giri, and S. Schiller, Test of charged baryon interaction with high-resolution vibrational spectroscopy of molecular hydrogen ions, Nat. Phys. **19**, 1263 (2023).

[5] D. Kliukin, V. Barbé, T. Klijn Velderman, J. B. E. Schokking, J. John, K. S. E. Eikema, J. C. J. Koelemeij, and J.-Ph. Karr, Spectroscopy of the hyperfine structure of HD^+ in rotationally excited states with 10-ppb uncertainty, arXiv:2608.00607 [physics.atom-ph].

[6] C. M. König, M. Bohman, F. Heiße, J. Morgner, T. Sailer, B. Tu, K. Blaum, S. Sturm, D. Bakalov, H. D. Nogueira, J.-Ph. Karr, O. Kullie, and S. Schiller, High-precision Penning trap spectroscopy of the ground state spin structure of HD^+, Phys. Rev. Lett. **136**, 143002 (2026).

[7] U. Bressel, A. Borodin, J. Shen, M. Hansen, I. Ernsting, and S. Schiller, Manipulation of individual hyperfine states in cold trapped molecular ions and application to HD^+ frequency metrology, Phys. Rev. Lett. **108**, 183003 (2012).

[8] J. Biesheuvel, J.-Ph. Karr, L. Hilico, K. S. E. Eikema, W. Ubachs, and J. C. J. Koelemeij, Probing QED and fundamental constants through laser spectroscopy of vibrational transitions in HD^+, Nat. Commun. **7**, 10385 (2016).

[9] A. Carrington, I. R. McNab, C. A. Montgomerie-Leach, and R. A. Kennedy, Vibration-rotation spectroscopy of the HD^+ ion near the dissociation limit: Part VI. Nuclear hyperfine interactions, Mol. Phys. **72**, 735 (1991).

[10] V. I. Korobov, L. Hilico, and J.-Ph. Karr, Fundamental transitions and ionization energies of the hydrogen molecular ions with few ppt uncertainty, Phys. Rev. Lett. **118**, 233001 (2017).

[11] V. I. Korobov and J.-Ph. Karr, Rovibrational spin-averaged transitions in the hydrogen molecular ions, Phys. Rev. A **104**, 032806 (2021).

[12] P. J. Mohr, D. B. Newell, B. N. Taylor, and E. Tiesinga, CODATA recommended values of the fundamental physical constants: 2022, Rev. Mod. Phys. **97**, 025002 (2025).

[13] J.-Ph. Karr and J. C. J. Koelemeij, Extraction of spin-averaged rovibrational transition frequencies in HD^+ for the determination of fundamental constants, Mol. Phys. **121**, e2216081 (2023).

[14] M. Germann, S. Patra, J.-Ph. Karr, L. Hilico, V. I. Korobov, E. J. Salumbides, K. S. E. Eikema, W. Ubachs, and J. C. J. Koelemeij, Three-body QED test and fifth-force constraint from vibrations and rotations of HD^+, Phys. Rev. Research **3**, L022028 (2021).

[15] C. Delaunay, J.-Ph. Karr, T. Kitahara, J. C. J. Koelemeij, Y. Soreq, and J. Zupan, Self-consistent extraction of spectroscopic bounds on light new physics, Phys. Rev. Lett. **130**, 121801 (2023).

[16] M. Haidar, V. I. Korobov, L. Hilico, and J.-Ph. Karr, Higher-order corrections to the spin-orbit and spin-spin tensor interactions in HD^+, Phys. Rev. A **106**, 042815 (2022).

[17] V. Patkóš, V. A. Yerokhin, and K. Pachucki, Higher-order QED corrections to the hyperfine splitting in ^{3}He, Phys. Rev. Lett. **131**, 183001 (2023).

[18] D. Bakalov, V. I. Korobov, and S. Schiller, High-precision calculation of the hyperfine structure of the HD^+ ion, Phys. Rev. Lett. **97**, 243001 (2006).

[19] V. I. Korobov, J. C. J. Koelemeij, L. Hilico, and J.-Ph. Karr, Theoretical hyperfine structure of the molecular hydrogen ion at the 1 ppm level, Phys. Rev. Lett. **116**, 053003 (2016).

[20] V. I. Korobov, J.-Ph. Karr, M. Haidar, and Z.-X. Zhong, Hyperfine structure in the H_2^+ and HD^+ molecular ions at order $m\alpha^6$, Phys. Rev. A **102**, 022804 (2020).

[21] J.-Ph. Karr, M. Haidar, L. Hilico, Z.-X. Zhong, and V. I. Korobov, Higher-order corrections to spin-spin scalar interactions in HD^+ and H_2^+, Phys. Rev. A **102**, 052827 (2020).

[22] M. Pańtak, V. Patkóš, and K. Pachucki, Nonrelativistic wave function of the hydrogen molecular ion (unpublished).

[23] K. Pachucki and J. Komasa, Leading order nonadiabatic corrections to rovibrational levels of H_2, D_2, and T_2, J. Chem. Phys. **143**, 034111 (2015).

[24] Z.-X. Zhong, P. Yang, V. I. Korobov, C. Li, and T.-Y. Shi, QED corrections of orders $m\alpha^6$ and $m\alpha^6(m/M)$ for HD^+ spin-independent rovibrational transitions beyond Born-Oppenheimer approximation, Phys. Rev. A **114**, 032814 (2026).

[25] L. Essen, R. W. Donaldson, E. G. Hope, and M. J. Bangham, Frequency of the hydrogen maser, Nature **229**, 110 (1971).

[26] L. Essen, R. W. Donaldson, E. G. Hope, and M. J. Bangham, Hydrogen maser work at the National Physical Laboratory, Metrologia **9**, 128 (1973).

[27] D. J. Wineland and N. F. Ramsey, Atomic deuterium maser, Phys. Rev. A **5**, 821 (1972).
[28] F. M. Fernández and J. Garcia, Highly accurate potential energy curves for the hydrogen molecule ion, ChemistrySelect **6**, 9527 (2021).
[29] Ts. Tsogbayar and V. I. Korobov, Relativistic correction to the $1s\sigma$ and $2p\sigma$ electronic states of the H_2^+ molecular ion and the moleculelike states of the antiprotonic helium $He^+\bar{p}$, J. Chem. Phys. **125**, 024308 (2006).
[30] D. M. Bishop and L. M. Cheung, Radiative corrections for the hydrogen molecular ion HD^+, J. Chem. Phys. **75**, 3155 (1981).
[31] R. Bukowski, B. Jeziorski, R. Moszyński, and W. Kołos, Bethe logarithm and Lamb shift for the hydrogen molecular ion, Int. J. Quantum Chem. **42**, 287 (1992).
[32] V. I. Korobov, Ro-vibrational states of H_2^+. Variational calculations, Mol. Phys. **116**, 93 (2018).
[33] M. I. Eides, H. Grotch, and V. A. Shelyuto, Theory of light hydrogenlike atoms, Phys. Rep. **342**, 63 (2001).
[34] K. Pachucki, $\alpha(Z\alpha)^2 E_F$ correction to hyperfine splitting in hydrogenic atoms, Phys. Rev. A **54**, 1994 (1996).
[35] V. Patkóš, V. A. Yerokhin, and K. Pachucki, Nuclear polarizability effects in $^3He^+$ hyperfine splitting, Phys. Rev. A **107**, 052802 (2023), Appendix A.
[36] K. Pachucki, Long-wavelength quantum electrodynamics, Phys. Rev. A **69**, 052502 (2004).
[37] D. T. Aznabayev, A. K. Bekbaev, and V. I. Korobov, Leading-order relativistic corrections to the rovibrational spectrum of H_2^+ and HD^+ molecular ions, Phys. Rev. A **99**, 012501 (2019).
[38] Z.-X. Zhong, P.-P. Zhang, Z.-C. Yan, and T.-Y. Shi, Precision spectroscopy of the hydrogen molecular ion HD^+, Phys. Rev. A **86**, 064502 (2012).
[39] V. I. Korobov, Bethe logarithm for the hydrogen molecular ion HD^+, Phys. Rev. A **70**, 012505 (2004).
[40] V. I. Korobov, Leading-order relativistic and radiative corrections to the rovibrational spectrum of H_2^+ and HD^+ molecular ions, Phys. Rev. A **74**, 052506 (2006).
[41] V. I. Korobov, L. Hilico, and J.-Ph. Karr, Calculation of the relativistic Bethe logarithm in the two-center problem, Phys. Rev. A **87**, 062506 (2013).
[42] D. T. Colbert and W. H. Miller, A novel discrete variable representation for quantum mechanical reactive scattering via the S-matrix Kohn method, J. Chem. Phys. **96**, 1982 (1992).
[43] E. A. Hylleraas, Über die Elektronenterme des Wasserstoffmoleküls, Z. Phys. **71**, 739 (1931).
[44] G. Jaffé, Zur Theorie des Wasserstoffmolekülions, Z. Phys. **87**, 535 (1934).
[45] W. G. Baber and H. R. Hassé, The two centre problem in wave mechanics, Proc. Cambridge Philos. Soc. **31**, 564 (1935).
[46] D. R. Bates, K. Ledsham, and A. L. Stewart, Wave functions of the hydrogen molecular ion, Phil. Trans. R. Soc. A **246**, 215 (1953).
[47] M. M. Madsen and J. M. Peek, Eigenparameters for the lowest twenty electronic states of the hydrogen molecule ion, At. Data **2**, 171 (1971).

Appendix A: Derivation of $\mathcal{A}_{e\gamma}^{(7)}$

In this Appendix we derive the three parts of $\mathcal{A}_{e\gamma}^{(7)}$ in Eq. (74) and transform them into the final form presented in Sec. IX.

1. Low-energy contribution

In the low-energy region the momentum k of the virtual photon is of the order of α^2. The corresponding low-energy contribution $\mathcal{A}_L^{(7)}$,

$$\mathcal{A}_L^{(7)} = \frac{2}{3}\int_0^\lambda dk\,\tilde{f}_\gamma(k)\,, \tag{A1}$$

is given by the perturbation of $-f$ in Eq. (29) by $\mathcal{V}_\gamma$,

$$\mathcal{V}_\gamma = \frac{4}{3}\,\pi\,\delta^{(3)}(r_\gamma)\,, \tag{A2}$$

where

$$\tilde{f}_\gamma(k) = 2\left\langle \mathcal{V}_\gamma \frac{1}{(\mathcal{E}-\mathcal{H})'}\,\vec{p}\,\frac{k}{\mathcal{E}-\mathcal{H}-k}\,\vec{p}\right\rangle + \left\langle \vec{p}\,\frac{k}{\mathcal{E}-\mathcal{H}-k}\,\big[\mathcal{V}_\gamma - \langle\mathcal{V}_\gamma\rangle\big]\,\frac{1}{\mathcal{E}-\mathcal{H}-k}\,\vec{p}\right\rangle, \tag{A3}$$

and $\vec{p}$ is the electron momentum operator. The large-k expansion of $\tilde{f}_\gamma(k)$ is

$$\tilde{f}_\gamma(k) = a_\gamma + \frac{b_\gamma}{\sqrt{k}} + \frac{c_\gamma\,\ln k}{k} + \frac{d_\gamma}{k} + \dots\,, \tag{A4}$$

where a_γ, b_γ, c_γ, and d_γ are the following coefficients:

$$a_\gamma = -\frac{2}{3}\left\langle \vec{p}^{\,2}\,\frac{1}{(\mathcal{E}-\mathcal{H})'}\,4\,\pi\,\delta^{(3)}(r_\gamma)\right\rangle, \tag{A5}$$

$$b_\gamma = -\frac{16\sqrt{2}}{3}\,\langle\pi\,\delta^{(3)}(r_\gamma)\rangle\,, \tag{A6}$$

$$c_\gamma = -\frac{8}{3}\,\langle\pi\,\delta^{(3)}(r_\gamma)\rangle\,, \tag{A7}$$

and

$$d_\gamma = \frac{1}{3}\left[\langle\vec{p}\,4\,\pi\,\delta^{(3)}(r_\gamma)\,\vec{p}\,\rangle + 4\left\langle 4\,\pi\,\delta^{(3)}(r_\gamma)\right\rangle\left\langle\frac{1}{r_A}+\frac{1}{r_B}\right\rangle - 2\left(\frac{3}{R}+\mathcal{E}\right)\left\langle 4\,\pi\,\delta^{(3)}(r_\gamma)\right\rangle + 2\left\langle\frac{\vec{r}_\gamma}{r_\gamma^3}\cdot\left(\frac{\vec{r}_A}{r_A^3}+\frac{\vec{r}_B}{r_B^3}\right)\right\rangle + \left\langle 4\,\pi\,[\delta^{(3)}(r_\gamma)]'\,\frac{1}{(\mathcal{E}-\mathcal{H})'}\,4\,\pi\,[\delta^{(3)}(r_A)+\delta^{(3)}(r_B)]'\right\rangle + 2\,(6-5\,\ln 2)\,\langle 4\,\pi\,\delta^{(3)}(r_\gamma)\rangle\right]. \tag{A8}$$

The λ-dependent part of $\mathcal{A}_L^{(7)}$ is separated as

$$\mathcal{A}_L^{(7)} = \mathcal{A}_{L'}^{(7)} + \frac{2}{3}\left(a_\gamma\,\lambda + 2\,b_\gamma\,\sqrt{\lambda} + \frac{c_\gamma}{2}\ln^2\lambda + d_\gamma\,\ln\lambda\right). \tag{A9}$$

Let $t = 1/\sqrt{1+2\,k}$, $t_\lambda = 1/\sqrt{1+2\,\lambda}$, and $f_\gamma(t) = \tilde{f}_\gamma(k)$; then

$$\begin{aligned}\mathcal{A}_{L'}^{(7)} &= \frac{2}{3}\lim_{\lambda\to\infty}\left[\int_{t_\lambda}^1 dt\,\frac{f_\gamma(t)}{t^3} - \left(a_\gamma\,\lambda + 2\,b_\gamma\,\sqrt{\lambda} + \frac{c_\gamma}{2}\ln^2\lambda + d_\gamma\,\ln\lambda\right)\right]\\ &= \frac{2}{3}\left[\int_0^1 dt\,\frac{f_\gamma(t) - a_\gamma - \sqrt{2}\,b_\gamma\,t + 2\,c_\gamma\,\ln(2\,t^2)\,t^2 - 2\,d_\gamma\,t^2}{t^3} - \sqrt{2}\,b_\gamma - \frac{c_\gamma}{2}\,\ln^2 2 + d_\gamma\,\ln 2\right].\end{aligned} \tag{A10}$$

Its numerical calculation is described in Appendix B.

2. Second-order contribution

The second-order contribution $E_{\rm sec}^{(7)}$ is

$$\begin{aligned}E_{\rm sec}^{(7)} &= 2\left\langle H_{{\rm hfs},A}^{(4)}\frac{1}{(E-H)'}\,H_A^{(5)}\right\rangle + 2\left\langle \kappa\,H_{{\rm hfs},A}^{(4)}\frac{1}{(E-H)'}\,H_A^{(4)}\right\rangle + 2\left\langle H_{{\rm hfs},B}^{(4)}\frac{1}{(E-H)'}\,2\,\kappa\,H_B^{(4)}\right\rangle\\ &= \sum_\gamma\left[\mathcal{A}_{e\gamma1}^{(7)} + \mathcal{A}_{e\gamma2}^{(7)} + \mathcal{A}_{e\gamma3}^{(7)}\right]\frac{\alpha}{\pi}\,(Z\,\alpha)^6\,\frac{m^2}{M_\gamma}\,g_\gamma\,\vec{I}_\gamma\cdot\vec{s}_e\,,\end{aligned} \tag{A11}$$

where $\kappa\,H_{{\rm hfs},A}^{(4)}$ is the part of Eq. (54) proportional to κ, and $H^{(5)}$ is the QED Hamiltonian

$$H^{(5)} = H_A^{(5)} + 2\,\kappa\,H_B^{(4)}\,, \tag{A12}$$

$$H_A^{(5)} = \left(\frac{5}{6} - \frac{1}{5} + \ln\frac{\alpha^{-2}}{2\lambda}\right)\frac{4\alpha^2 Z}{3m^2}\left[\delta^{(3)}(r_A) + \delta^{(3)}(r_B)\right], \tag{A13}$$

where $\kappa = \alpha/(2\,\pi)$. Thus,

$$\mathcal{A}_{e\gamma1}^{(7)} = 2\left\langle\frac{4}{3}\,\pi\,\delta^{(3)}(r_\gamma)\frac{1}{(\mathcal{E}-\mathcal{H})'}\left(\frac{5}{6} - \frac{1}{5} + \ln\frac{\alpha^{-2}}{2\lambda}\right)\frac{4}{3}\,\pi\left[\delta^{(3)}(r_A) + \delta^{(3)}(r_B)\right]\right\rangle, \tag{A14}$$

$$\mathcal{A}_{e\gamma2}^{(7)} = \frac{1}{3}\left\langle 4\,\pi\,\delta^{(3)}(r_\gamma)\,\frac{1}{(\mathcal{E}-\mathcal{H})'}\left(-\frac{p^4}{8} + \frac{\pi}{2}\left[\delta^{(3)}(r_A) + \delta^{(3)}(r_B)\right]\right)\right\rangle = \frac{1}{2}\,\mathcal{A}_{e\gamma2}^{(6)}\,, \tag{A15}$$

$$\mathcal{A}_{e\gamma3}^{(7)} = \frac{1}{6}\left\langle\frac{\vec{r}_\gamma}{r_\gamma^3}\times\vec{p}\,\frac{1}{\mathcal{E}-\mathcal{H}}\left(\frac{\vec{r}_A}{r_A^3} + \frac{\vec{r}_B}{r_B^3}\right)\times\vec{p}\right\rangle = \mathcal{A}_{e\gamma3}^{(6)}\,. \tag{A16}$$

The singularities in these second-order matrix elements cancel with those of the first-order matrix elements.

3. First-order contribution

The effective Hamiltonian $H_{\rm hfs}^{(7)}$ of order $m\alpha^7$ can be represented as

$$\begin{aligned}\langle H_{\rm hfs}^{(7)}\rangle &= \langle H_{{\rm hfs},A}^{(7)} + H_{{\rm hfs},B}^{(7)} + \sum_\gamma\zeta_\gamma\,\frac{\alpha}{\pi}\,\frac{(Z\,\alpha)^3}{m\,M_\gamma}\,g_\gamma\,\pi\,\delta^{(3)}(r_\gamma)\,\vec{I}_\gamma\cdot\vec{s}_e\rangle\\ &= \sum_\gamma\left[A_{e\gamma A}^{(7)} + A_{e\gamma B}^{(7)} + \zeta_\gamma\,\frac{\alpha}{\pi}\,\frac{(Z\,\alpha)^3}{m\,M_\gamma}\,g_\gamma\,\langle\pi\,\delta^{(3)}(r_\gamma)\rangle\right]\vec{I}_\gamma\cdot\vec{s}_e\,,\end{aligned} \tag{A17}$$

where ζ_γ accounts for terms that are proportional to $\delta^{(3)}(r_\gamma)$; it is assumed to be independent of R and is obtained by matching with the hydrogenic result. In the first stage of the derivation we routinely drop such terms; the corresponding contribution is restored later by matching to the known hydrogenic result; see Sec. A 4. More specifically, we omit terms proportional to $Z^3\,\delta^{(3)}(r_\gamma)$; all other terms proportional to $\delta^{(3)}(r_\gamma)$ are preserved throughout the derivation.

The first part, $H^{(7)}_{\rm hfs,A}$, comes from the spin-dependent terms in the FW Hamiltonian $H_{\rm FW}$ [36] that are proportional to the electron anomalous magnetic moment κ. Specifically,

$$\delta_\kappa H_{\rm FW} = \kappa \left\{ \sum_\beta \frac{Z\alpha}{2\,m^2}\,\vec\sigma\cdot\frac{\vec r_\beta}{r_\beta^3}\times\vec\pi + \frac{e}{8\,m^3}\,\{\vec\pi\cdot\vec B\,,\,\vec\pi\cdot\vec\sigma\} + \frac{e}{16\,m^3}\,[\pi^i\,,\,[\pi^i\,,\,\vec\sigma\cdot\vec B]] \right\}, \tag{A18}$$

so that

$$H^{(7)}_{\rm hfs,A} = \sum_\gamma \kappa \left[\sum_\beta \frac{Z\alpha}{2\,m^2}\,\vec\sigma\cdot\frac{\vec r_\beta}{r_\beta^3}\times\big(-e\vec A_\gamma\big) + \frac{e}{4\,m^3}\,(\vec p\cdot\vec\sigma)(\vec B_\gamma\cdot\vec p) - \frac{e}{16\,m^3}\,\vec\sigma\cdot\Delta\vec B_\gamma \right]. \tag{A19}$$

Using $\vec A_\gamma(\vec r)$ and $B^i_\gamma(\vec r)$ given in Eqs. (58) and (59), we obtain

$$\begin{aligned} A^{(7)}_{e\gamma A} = {}& \frac{g_\gamma\,Z\alpha\,\kappa}{2\,M_\gamma}\left\langle \frac{2Z\alpha}{3\,m^2}\,\frac{\vec r_\gamma}{r_\gamma^3}\cdot\left(\frac{\vec r_A}{r_A^3}+\frac{\vec r_B}{r_B^3}\right)\right. \\ & \left. - \frac{1}{6\,m^3}\left(\frac{8\pi}{3}\,p^i\,\delta^{(3)}(r_\gamma)\,p^i - p^i\,\frac{1}{r_\gamma^5}\big(r_\gamma^2\,\delta^{ij}-3\,r_\gamma^i r_\gamma^j\big)\,p^j\right) + \frac{\pi}{3\,m^3}\,\Delta\,\delta^{(3)}(r_\gamma)\right\rangle. \end{aligned} \tag{A20}$$

The second part of $H^{(7)}_{\rm hfs}$ is the middle-energy contribution, which can be expressed in terms of the slopes of the form factors and the one-loop vacuum polarization,

$$H^{(7)}_{\rm hfs,B} = \sum_\gamma -\frac{e}{2\,m}\left[F_1'(0)+F_2'(0)-\frac{\alpha}{15\,\pi\,m^2}\right]\vec\sigma\cdot\Delta\,\vec B_\gamma\,, \tag{A21}$$

and thus

$$A^{(7)}_{e\gamma B} = \frac{4\pi}{3}\,\frac{g_\gamma\,Z\alpha}{m^3\,M_\gamma}\left[\frac{17}{72}+\frac{1}{3}\ln\frac{\alpha^{-2}}{2\lambda}-\frac{1}{15}\right]\frac{\alpha}{\pi}\,\langle\Delta\,\delta^{(3)}(r_\gamma)\rangle\,, \tag{A22}$$

where the slopes of the form factors are given by

$$F_1'(0)+F_2'(0) = \frac{\alpha}{\pi\,m^2}\left[\frac{17}{72}+\frac{1}{3}\ln\frac{\alpha^{-2}}{2\lambda}\right]. \tag{A23}$$

4. Elimination of λ and divergences from the first-order terms, and matching with hydrogen

The total result for $\mathcal{A}^{(7)}_{e\gamma}$ corresponding to Eq. (74) is of the form

$$\mathcal{A}^{(7)}_{e\gamma} = \mathcal{A}^{(7)}_{L} + \mathcal{A}^{(7)}_{e\gamma 1} + \mathcal{A}^{(7)}_{e\gamma 2} + \mathcal{A}^{(7)}_{e\gamma 3} + \mathcal{A}^{(7)}_{e\gamma A} + \mathcal{A}^{(7)}_{e\gamma B} + \zeta_\gamma\,\langle\pi\delta^{(3)}(r_\gamma)\rangle\,. \tag{A24}$$

The second-order matrix elements $\mathcal{A}^{(7)}_{e\gamma 1}$ and $\mathcal{A}^{(7)}_{e\gamma 2}$ contain divergences. They are moved to the first-order matrix elements using Eqs. (68), (69), and (71). Applying these identities, we obtain

$$\begin{aligned} \mathcal{A}^{(7)}_{e\gamma 1} = {}& \frac{2}{9}\left(\frac{5}{6}-\frac{1}{5}+\ln\frac{\alpha^{-2}}{2\lambda}\right)\left\{\left\langle 4\,\pi\,[\delta^{(3)}(r_\gamma)]'\,\frac{1}{(\mathcal{E}-\mathcal{H})'}\,4\,\pi\,[\delta^{(3)}(r_A)+\delta^{(3)}(r_B)]'\right\rangle + 4\left\langle\left(\frac{1}{r_A}+\frac{1}{r_B}\right)\right\rangle\langle 4\,\pi\,\delta^{(3)}(r_\gamma)\rangle\right. \\ & \left. - 4\left\langle\left(\frac{1}{r_A}+\frac{1}{r_B}\right)4\,\pi\,\delta^{(3)}(r_\gamma)\right\rangle + 2\left\langle\frac{\vec r_\gamma}{r_\gamma^3}\cdot\left(\frac{\vec r_A}{r_A^3}+\frac{\vec r_B}{r_B^3}\right)\right\rangle\right\}, \end{aligned} \tag{A25}$$

$$\begin{aligned} \mathcal{A}^{(7)}_{e\gamma 2} = {}& \frac{1}{3}\left\{\left\langle 4\,\pi\,[\delta^{(3)}(r_\gamma)]'\,\frac{1}{(\mathcal{E}-\mathcal{H})'}\,\mathcal{H}_A'^{(4)}\right\rangle + 2\left\langle\frac{1}{r_\gamma}\right\rangle\mathcal{E}^{(4)} - \langle\pi\,\delta^{(3)}(r_\gamma)\rangle\left\langle\frac{1}{r_A}+\frac{1}{r_B}\right\rangle\right. \\ & \left. + \frac{1}{4}\left\langle\frac{\vec r_\gamma}{r_\gamma^3}\cdot\left(\frac{\vec r_A}{r_A^3}+\frac{\vec r_B}{r_B^3}\right)\right\rangle + \left\langle\frac{1}{r_\gamma}\left(\mathcal{E}+\frac{1}{r_A}+\frac{1}{r_B}\right)^2\right\rangle\right\}. \end{aligned} \tag{A26}$$

The total result is now written in the form

$$\mathcal{A}^{(7)}_{e\gamma} = \mathcal{A}^{(7)}_{L'} + \mathcal{A}^{(7)}_{\rm sec} + \mathcal{A}^{(7)}_{\rm fo}\,. \tag{A27}$$

The $\ln\lambda$ terms cancel out in $\mathcal{A}^{(7)}_{\rm fo}$, and, shifting the terms proportional to $\langle\pi\delta^{(3)}(r_\gamma)\rangle$ to ζ_γ, we obtain

$$\begin{aligned}\mathcal{A}^{(7)}_{\rm fo} &= \frac{2}{9}\left(\frac{5}{6}-\frac{1}{5}+\ln\frac{\alpha^{-2}}{2}\right)\left[4\left\langle\left(\frac{1}{r_A}+\frac{1}{r_B}\right)\right\rangle\langle 4\,\pi\,\delta^{(3)}(r_\gamma)\rangle-\frac{4}{R}\left\langle 4\,\pi\,\delta^{(3)}(r_\gamma)\right\rangle+2\left\langle\frac{\vec r_\gamma}{r_\gamma^3}\cdot\left(\frac{\vec r_A}{r_A^3}+\frac{\vec r_B}{r_B^3}\right)\right\rangle\right]\\ &+\frac{1}{3}\left[2\left\langle\frac{1}{r_\gamma}\right\rangle\mathcal{E}^{(4)}-\langle\pi\,\delta^{(3)}(r_\gamma)\rangle\left\langle\frac{1}{r_A}+\frac{1}{r_B}\right\rangle+\frac{1}{4}\left\langle\frac{\vec r_\gamma}{r_\gamma^3}\cdot\left(\frac{\vec r_A}{r_A^3}+\frac{\vec r_B}{r_B^3}\right)\right\rangle+\left\langle\frac{1}{r_\gamma}\left(\mathcal{E}+\frac{1}{r_A}+\frac{1}{r_B}\right)^2\right\rangle\right]\\ &+\frac{1}{4}\left\langle\frac{2}{3}\frac{\vec r_\gamma}{r_\gamma^3}\cdot\left(\frac{\vec r_A}{r_A^3}+\frac{\vec r_B}{r_B^3}\right)-\frac{1}{6}\frac{8\pi}{3}\,\vec p\,\delta^{(3)}(r_\gamma)\,\vec p+\frac{1}{6}\,p^i\,\frac{1}{r_\gamma^5}\left(r_\gamma^2\,\delta^{ij}-3\,r_\gamma^i r_\gamma^j\right)p^j+\frac{\pi}{3}\,\Delta\,\delta^{(3)}(r_\gamma)\right\rangle\\ &+\frac{4}{3}\left[\frac{17}{72}+\frac{1}{3}\ln\frac{\alpha^{-2}}{2}-\frac{1}{15}\right]\langle\pi\,\Delta\,\delta^{(3)}(r_\gamma)\rangle+\zeta_\gamma\,\langle\pi\delta^{(3)}(r_\gamma)\rangle\,. \end{aligned}\tag{A28}$$

Some operators can be simplified further; the relevant identities, valid up to terms proportional to $\delta^{(3)}(r)$, are

$$\langle 4\,\pi\,\Delta\delta^{(3)}(r_\gamma)\rangle = 2\,\langle\vec p\,4\,\pi\,\delta^{(3)}(r_\gamma)\,\vec p\rangle-4\left(\mathcal{E}+\frac{1}{R}\right)\langle 4\,\pi\,\delta^{(3)}(r_\gamma)\rangle\,,\tag{A29}$$

$$\left\langle p^i\,\frac{1}{r_\gamma^3}\left(\delta^{ij}-3\frac{r_\gamma^i r_\gamma^j}{r_\gamma^2}\right)p^j\right\rangle=\left\langle\frac{2}{3}\,\vec p\,\pi\,\delta^{(3)}(r_\gamma)\,\vec p+\frac{\vec r_\gamma}{r_\gamma^3}\cdot\left(\frac{\vec r_A}{r_A^3}+\frac{\vec r_B}{r_B^3}\right)-\left(\mathcal{E}+\frac{1}{R}\right)4\,\pi\delta^{(3)}(r_\gamma)\right\rangle.\tag{A30}$$

Using the identities (A29) and (A30) and matching with hydrogen (see Ref. [34] and Appendix A of Ref. [35]), we obtain $\mathcal{A}^{(7)}_{\rm fo}$ as given in Eq. (81), with the regularized matrix elements defined in Eqs. (76)–(80).

Appendix B: Technical details of the numerical calculations for HD^+

The numerical results for $\mathcal{E}^{(2)}$, $\mathcal{E}^{(4)}$, $\mathcal{E}^{(5)}$, $\mathcal{A}^{(4)}_{e\gamma}$, $\mathcal{A}^{(6)}_{e\gamma}$, and $\mathcal{A}^{(7)}_{e\gamma}$ on a predefined grid of R are presented in Table VIII. The large-R limits of $\mathcal{E}^{(i)}$ are equal to the hydrogenic values and are given in Eqs. (13), (24), and (38), while those of $\mathcal{A}^{(i)}_{e\gamma}$ are equal to half of the hydrogenic values; see Eqs. (15), (73), and (88). The numerical values of all these limits are shown in the last row of Table VIII. Below we present technical details of the numerical calculations performed in this work, which exploit the separability of the two-center Schrödinger equation.

1. Two-center Schrödinger equation

The two-center Schrödinger equation (10) is separable in the prolate spheroidal coordinates [43–45]

$$\xi=\frac{r_A+r_B}{R}\,,\tag{B1}$$

$$\eta=\frac{r_A-r_B}{R}\,.\tag{B2}$$

Consequently, the wave function of the ground electronic state is of the form

$$\phi(\xi,\eta)=\Lambda(\xi)\,M(\eta)\,,\tag{B3}$$

where Λ and M satisfy the following differential equations

$$\frac{d}{d\xi}\left[(\xi^2-1)\,\frac{d\Lambda}{d\xi}\right]+\left(A+2\,R\,\xi-p^2\,\xi^2\right)\Lambda=0\,,\tag{B4}$$

$$\frac{d}{d\eta}\left[(1-\eta^2)\,\frac{dM}{d\eta}\right]+\left(-A+p^2\,\eta^2\right)M=0\,,\tag{B5}$$

A is the separation constant, and

$$p^2=-\frac{\mathcal{E}\,R^2}{2}\,.\tag{B6}$$

The function M is expanded in the Legendre polynomials with even l,

$$M(\eta)=\sum_l c_l\,P_l(\eta)\,,\tag{B7}$$

and for Λ we use the expansion of Jaffé [44],

$$\Lambda(\xi)=e^{-p\,\xi}\,(\xi+1)^{R/p-1}\sum_n g_n\left(\frac{\xi-1}{\xi+1}\right)^n.\tag{B8}$$

The coefficients c_l and g_n satisfy three-term recurrence relations, and the requirement that both of them have solutions with the same A determines p, and thus the energy $\mathcal{E}(R)$ [46, 47]. We solve these equations in arbitrary-precision arithmetic, so that $\mathcal{E}(R)$ and the wave function are obtained with more than 30 significant digits. As a check, our result at the equilibrium distance $R=2$ is in perfect agreement with the result of Ref. [28], which is accurate to more than 100 digits.

2. First-order matrix elements

The first-order matrix elements in $\mathcal{E}^{(4)}$, $\mathcal{E}^{(5)}$, $\mathcal{A}^{(6)}_{e\gamma}$, and $\mathcal{A}^{(7)}_{\rm fo}$, including the regularized ones in Eqs. (76) and (77),

are calculated by direct numerical integration with this exact wave function. In the spheroidal coordinates of Eqs. (B1) and (B2)

$$r_A = \frac{R}{2}\,(\xi+\eta)\,, \tag{B9}$$

$$r_B = \frac{R}{2}\,(\xi-\eta)\,, \tag{B10}$$

$$d^3r = \frac{R^3}{8}\,(\xi^2-\eta^2)\,d\xi\,d\eta\,d\varphi\,, \tag{B11}$$

so that these matrix elements are two-dimensional integrals over $\xi \in (1,\infty)$ and $\eta \in (-1,1)$. The differential operators are eliminated beforehand with the help of the Schrödinger equation (10), for example

$$\langle p^4 \rangle = 4\left\langle \left(\mathcal{E} + \frac{1}{r_A} + \frac{1}{r_B}\right)^2 \right\rangle, \tag{B12}$$

and the expectation value of the Dirac δ function, for ϕ normalized to unity, is

$$\langle \delta^{(3)}(r_\gamma) \rangle = \phi^2(1,\eta_\gamma)\,, \tag{B13}$$

where $\eta_A = -1$ and $\eta_B = 1$. In $\mathcal{E}^{(4)}$ and $\mathcal{A}^{(6)}_{e\gamma}$ the factors $(\xi \pm \eta)^{-1}$ are expanded according to Eq. (B28) below. The integral over η is then performed analytically with the Legendre expansion of the η-dependent part of the integrand, and the remaining integral over ξ is evaluated by an adaptive quadrature in arbitrary-precision arithmetic. In $\mathcal{A}^{(7)}_{\rm fo}$ the matrix elements with integrable singularities, $\langle 1/(r_A\,r_B)\rangle$, $\langle 1/(r_A^2\,r_B)\rangle$, and $\langle \vec{r}_A\cdot\vec{r}_B/(r_A^3\,r_B^3)\rangle$, are evaluated with the Gauss–Legendre quadrature in ξ and η on intervals graded geometrically towards the nuclei. For the regularized matrix elements in Eqs. (76) and (77) with $\gamma = A$ we use the variables $u = \xi+\eta = 2\,r_A/R$ and $v = \xi-\eta$, and first integrate over v,

$$g(u) = \int dv\, v\, \phi^2\,, \tag{B14}$$

where $|2-u| < v < 2+u$. The small-u expansion of this function is

$$g(u) = g_1\,u + g_2\,u^2 + O(u^3)\,, \tag{B15}$$

where $g_1 = 4\,\phi^2$ at the nucleus A and $g_2 = -R\,g_1$ follows from the cusp condition. These two terms are subtracted from $g(u)$ and integrated analytically with u^{-2} and u^{-3}, which gives the $\epsilon \to 0$ limit in Eqs. (76) and (77), while the remainder is integrated numerically. Finally, the matrix element in Eq. (80) is obtained from the nonspherical part of the gradient of ϕ at the nucleus,

$$\langle \vec{p}\,\delta^{(3)}(r_A)\,\vec{p}\,\rangle = \frac{1}{R^2}\left(\Lambda\,\frac{dM}{d\eta} - M\,\frac{d\Lambda}{d\xi}\right)^2\Bigg|_{\xi=1,\,\eta=-1}, \tag{B16}$$

and it vanishes in the hydrogenic limit. As a test, the normalization of ϕ, $\langle 1/r_A\rangle$, and $\langle 1/r_A^2\rangle$ obtained with these different integration schemes agree to better than 10^{-15} at all distances R. In comparison with previous calculations, the mass–velocity and Darwin terms of Ref. [29] give $\mathcal{E}^{(4)}$ within 8.1×10^{-11} of our values at the 13 common distances.

3. Bethe logarithm

The calculation of the Bethe logarithm requires the solution of the first-order equation

$$(\mathcal{H} - \mathcal{E} + k)\,\vec{\psi} = \vec{\nabla}\phi \tag{B17}$$

for all values of the photon momentum k. We again take advantage of the separability: for functions with the angular dependence $e^{\pm i\,m\,\varphi}$ around the internuclear axis, the operator

$$\frac{R^2}{2}\,(\xi^2-\eta^2)\,(\mathcal{H} - \mathcal{E} + k) = \mathcal{T}_\xi + \mathcal{T}_\eta\,, \tag{B18}$$

is a sum of an operator in ξ and an operator in η,

$$\mathcal{T}_\xi = -\frac{\partial}{\partial\xi}\,(\xi^2-1)\,\frac{\partial}{\partial\xi} + \frac{m^2}{\xi^2-1} - 2\,R\,\xi + q^2\,\xi^2\,, \tag{B19}$$

$$\mathcal{T}_\eta = -\frac{\partial}{\partial\eta}\,(1-\eta^2)\,\frac{\partial}{\partial\eta} + \frac{m^2}{1-\eta^2} - q^2\,\eta^2\,, \tag{B20}$$

where

$$q^2 = \frac{(k-\mathcal{E})\,R^2}{2}\,. \tag{B21}$$

Therefore, Eq. (B17) is solved in the product basis

$$\chi^m_{nl}(\xi,\eta) = (\xi^2-1)^{m/2}\,e^{-\beta\,(\xi-1)} \times L^{(m)}_n\big(2\,\beta\,(\xi-1)\big)\,P^m_l(\eta)\,, \tag{B22}$$

where $L^{(m)}_n$ are the associated Laguerre polynomials, P^m_l are the associated Legendre functions, $m = 0, 1$, and

$$\beta = \sqrt{p\,q}\,. \tag{B23}$$

The right-hand side of Eq. (B17) is calculated with the exact wave function ϕ of Eq. (B3), and its projections on the basis functions are obtained by the Gauss–Legendre quadrature in η and the Gauss–Laguerre quadrature in ξ. Since $(\xi^2-\eta^2)\,\vec{\nabla}\phi$ consists of two products of functions of ξ and of η, and the solution is analytic in both variables, the linear system reduces to a tridiagonal eigenvalue problem in l and banded systems in n, and the expansion converges exponentially.

Using quadruple-precision arithmetic, $f(t)$ of Eq. (29) is obtained with 25–30 significant digits. The integral over t in Eq. (27) is evaluated with the Gauss–Legendre quadrature on intervals graded towards $t = 0$ down to $t_0 \sim 10^{-3}$. For $t < t_0$ we use the expansion in Eq. (30), supplemented by terms t^n and $t^n \ln t$ up to $n = 12$, with coefficients fitted to the calculated values. The numerical fit reproduces f_3 and f_4 of Eqs. (33) and (34) to better than 10^{-10}, which gives us confidence in the accuracy of $f(t)$ for $t > t_0$.

One more factor has to be taken into account. At large R the state $1s\sigma_u$ with the wave function ϕ_u is nearly degenerate with the ground state. Its contribution to f,

$$f_u(t) = |\langle\phi_u|\vec{p}|\phi\rangle|^2\,\frac{k}{k+\Delta}\,, \tag{B24}$$

where Δ is the excitation energy, varies rapidly near $t = 1$. It is therefore subtracted from $f(t)$, and its contribution to the Bethe logarithm,

$$D\,\ln k_0\big|_u = |\langle\phi_u|\vec{p}\,|\phi\rangle|^2\,\Delta\,\ln(2\,\Delta)\,, \tag{B25}$$

is added analytically. We observe moderate agreement with the previous calculations of Ref. [41]. For example, Eq. (25) with our contact term and $\ln k_0$ from the Supplemental Material of Ref. [41] differs from our $\mathcal{E}^{(5)}$ by 2.6×10^{-5}, 4.4×10^{-10}, and 9.2×10^{-7} at $R = 0.1$, 2, and 7, respectively, while all our results are accurate to 10^{-12}.

4. Second-order matrix elements

In the second-order terms of $\mathcal{A}^{(6)}_{e\gamma}$ in Eq. (72) and of $\mathcal{A}^{(7)}_{e\gamma}$ in Eq. (83), both $4\,\pi\,[\delta^{(3)}(r_\gamma)]'\phi$ and $\mathcal{H}'^{(4)}_A\phi$ behave as r_γ^{-2} at the nucleus. Thus, the first-order wave function contains $\ln r_\gamma$, which cannot be represented efficiently by polynomials in ξ and η. Therefore, we use the fact that $(\xi^2-\eta^2)\,4\,\pi\,[\delta^{(3)}(r_A)]'\phi$ is equal to $(\xi+\eta)^{-2}$ times a sum of two products of functions of ξ and of η, and employ the integral representation

$$\frac{1}{(\xi+\eta)^2} = \int_0^\infty ds\,s\,e^{-s\,(\xi+\eta)}\,. \tag{B26}$$

The second-order matrix element with an arbitrary operator Q then becomes

$$\left\langle 4\,\pi\,[\delta^{(3)}(r_A)]'\,\frac{1}{(\mathcal{E}-\mathcal{H})'}\,Q\right\rangle = \int_0^\infty ds\,g(s)\,, \tag{B27}$$

where $g(s)$ involves the solution of the first-order equation with a source that is analytic in ξ and η. This equation is solved in the product basis of Eq. (B22) with $k = 0$ and with a single exponent for all values of s, chosen arbitrarily to be $\beta = \sqrt{2\,p\,s_{\max}}$, where $s_{\max}$ is the upper limit of the numerical integration over s and is a few hundred. Because the operator $\mathcal{H}-\mathcal{E}$ does not depend on s, the matrices and the projections of $Q\,\phi$ are calculated only once for each R, while the number of basis functions in ξ is increased to achieve high numerical precision.

The projections of $Q\,\phi$, namely of $\mathcal{H}'^{(4)}_A\phi$ or $(\vec{r}_A/r_A^3 + \vec{r}_B/r_B^3)\times\vec{p}\,\phi$, on the basis functions are obtained using the expansion

$$\frac{1}{\xi\pm\eta} = \sum_{l=0}^{\infty}(2\,l+1)\,(\mp1)^l\,Q_l(\xi)\,P_l(\eta)\,, \tag{B28}$$

where Q_l are the Legendre functions of the second kind (the terms with $(\xi\pm\eta)^{-2}$ are reduced to this form by integration by parts). The function $g(s)$ is calculated for $s \le s_{\max}$, and the integral over $s > s_{\max}$ is obtained from the expansion

$$g(s) = \sum_{n\ge2}\frac{a_n + b_n\,\ln s}{s^n}\,, \tag{B29}$$

with the coefficients fitted to the calculated values.

The last term in Eq. (72) is calculated in the same way. The operator $\vec{r}_\gamma/r_\gamma^3\times\vec{p}$ changes the symmetry of the wave function from σ to π, so that the first-order wave function is expanded in the basis functions χ^1_{nl} of Eq. (B22), and the resolvent does not require the subtraction of the ground state. For $\gamma = A$ we have

$$(\xi^2-\eta^2)\,\frac{\vec{r}_A}{r_A^3}\times\vec{\nabla}\phi = \frac{8}{R^3}\,\frac{\sqrt{(\xi^2-1)\,(1-\eta^2)}}{(\xi+\eta)^2} \times\left(\frac{d\Lambda}{d\xi}\,M - \Lambda\,\frac{dM}{d\eta}\right)\vec{e}_\varphi\,, \tag{B30}$$

where $\vec{e}_\varphi$ is the unit vector in the azimuthal direction around the internuclear axis, and the result for $\gamma = B$ is obtained by the replacement $\eta\to-\eta$. This source is again $(\xi+\eta)^{-2}$ times a sum of two products of functions of ξ and of η, and it behaves as r_A^{-2} at the nucleus. We therefore use the integral representation in Eq. (B26), and for each s solve the first-order equation with an analytic source in the same basis, with the same β and $s_{\max}$ as above. The projections of $(\vec{r}_A/r_A^3+\vec{r}_B/r_B^3)\times\vec{p}\,\phi$ on the basis functions χ^1_{nl} are obtained with the help of Eq. (B28), and the integral over $s > s_{\max}$ from the expansion in Eq. (B29).

5. Scalar hfs correction to the Bethe logarithm

The scalar hfs correction to the Bethe logarithm is calculated using the same product basis of Eq. (B22) with β from Eq. (B23) as for the ordinary Bethe logarithm. The function $\tilde{f}_\gamma(k)$ of Eq. (A3) is expressed in terms of the solution $\vec{\psi}$ of Eq. (B17) as

$$\tilde{f}_\gamma(k) = k\left[2\,\langle\phi|\mathcal{V}_\gamma|\psi\rangle + \langle\vec{\psi}\,|\mathcal{V}_\gamma - \langle\mathcal{V}_\gamma\rangle|\vec{\psi}\,\rangle\right], \tag{B31}$$

$$\psi = \frac{1}{(\mathcal{E}-\mathcal{H})'}\,\vec{\nabla}\cdot\vec{\psi}\,, \tag{B32}$$

where ϕ is normalized to unity. Since $(\xi^2-\eta^2)\,\vec{\nabla}\cdot\vec{\psi}$ is analytic in ξ and η, the function ψ is expanded in the basis functions χ^0_{nl} of Eq. (B22) with even l and with the same exponent β of Eq. (B23) as used for $\vec{\psi}$ at the given k. The equation for ψ is solved using Eq. (B18) at $k = 0$, and the reduced resolvent is obtained by projecting out the ground state represented in this basis. Because $\mathcal{V}_\gamma$ of Eq. (A2) is proportional to $\delta^{(3)}(r_\gamma)$,

$$\langle\phi|\mathcal{V}_\gamma|\psi\rangle = \frac{4\,\pi}{3}\,\phi(1,\eta_\gamma)\,\psi(1,\eta_\gamma)\,, \tag{B33}$$

$$\langle\vec{\psi}\,|\mathcal{V}_\gamma|\vec{\psi}\,\rangle = \frac{4\,\pi}{3}\,|\vec{\psi}(1,\eta_\gamma)|^2\,, \tag{B34}$$

as in Eq. (B13). These values are calculated directly from the expansions in the basis functions. No regularization of $\mathcal{V}_\gamma$ is needed here, because the functions ϕ, ψ, and $\vec{\psi}$ have only Coulomb cusps at the nuclei and are therefore analytic in ξ and η. The integral in Eq. (A10) is evaluated with the Gauss–Legendre quadrature on intervals graded towards $t = 0$ and

$t = 1$, down to $t_0 \sim 10^{-3}$–10^{-2}, and for $t < t_0$ the integrand is represented by the terms $t^n \ln^j t$ with $n \leq 4$ and $j \leq 2$, fitted to the calculated values.

6. DVR averaging

With all the potentials of Table VIII at hand, the radial equation for χ_{vL} is solved with the discrete variable representation of Colbert and Miller [42] and with the CODATA 2022 masses of Table VI. The potentials $\mathcal{E}^{(2)}(R)$, $\mathcal{A}^{(4)}_{e\gamma}(R)$, and $\mathcal{E}^{(4)}(R)$ are evaluated exactly on demand for the DVR averaging, while for $\mathcal{A}^{(6)}_{e\gamma}$, $\mathcal{A}^{(7)}_{e\gamma}$, and $\mathcal{E}^{(5)}$ the smooth ratios $\mathcal{A}^{(6)}_{e\gamma}/\mathcal{A}^{(4)}_{e\gamma}$, $\mathcal{A}^{(7)}_{e\gamma}/\mathcal{A}^{(4)}_{e\gamma}$, and $\mathcal{E}^{(5)}/\mathcal{A}^{(4)}_{e\gamma}$ are interpolated by splines in $\ln R$. With the DVR eigenvector components $\chi_{vL}(R_k)$ normalized as $\sum_k \chi^2_{vL}(R_k) = 1$, the first-order averages are

$$\Delta^{(i)}_{vL} = \sum_k \chi^2_{vL}(R_k)\, \tilde{\mathcal{A}}^{(i)}_{e\gamma}(R_k)\,, \tag{B35}$$

and the second-order ones

$$\delta^{(i)}_{vL} = 2 \sum_{n \neq v} \frac{\langle v, L|\mathcal{E}^{(i-2)}|n, L\rangle\langle n, L|\mathcal{A}^{(4)}_{e\gamma}|v, L\rangle}{\mathcal{E}_{vL} - \mathcal{E}_{nL}}\,, \tag{B36}$$

where the sum over the complete DVR spectrum for the same L represents the reduced resolvent; for $i = 7$ the term $\delta^{(6)}_{vL}/2$ of Eq. (46) is added. The averages are given in Table IX. δ and Δ are of the same order and tend to cancel in the sum.

Using the sums $\delta+\Delta$, we obtain $A^{(6)}_{e\gamma}$ and $A^{(7)}_{e\gamma}$ in Hz, which are presented in Tables X ($\gamma = p$) and XI ($\gamma = d$). For the ground state $A^{(6)}_{ep} = -7672.28$ Hz and $A^{(7)}_{ep} = -538.32$ Hz, of which $+17.68$ Hz comes from the anomalous magnetic moment. We note that $A^{(7)}_{ep}/A^{(6)}_{ep} = 0.07$ is much larger than the naive estimate of a single power of the fine-structure constant α. The dependence on v is a few percent per vibrational quantum, and that on L is about one percent over $L = 0$–3.

7. Nonadiabatic contact term

Tables X ($\gamma = p$) and XI ($\gamma = d$) list the nonadiabatic expectation values $\langle \pi\delta^{(3)}(r_{e\gamma})\rangle_{vL}$, obtained with the full three-body wave function [22] and the mass ratios of Table VI, the first term of Eq. (42), $\bar{A}_{ep}$ and $\bar{A}_{ed}$, and the totals A_{ep} and A_{ed}, which are collected by v and L in Table I. For the ground state, the nonadiabatic $\langle \pi\delta^{(3)}(r_{ep})\rangle_{00} = 0.650\,444$ lies 0.18% below the Born–Oppenheimer value $0.651\,633$, which is the expected finite-nuclear-mass effect. For $v \leq 4$ and $L \leq 3$, after accounting for the nuclear masses, the values of $\langle \pi\delta^{(3)}(r_{e\gamma})\rangle_{vL}$ in Tables X and XI agree, within the numerical precision quoted in these tables, with the results of Zhong *et al.* from Table II of Ref. [38].

The comparison with the earlier results of Aznabayev *et al.* [37] is more complicated. The values of $\langle \pi\delta^{(3)}(r_{e\gamma})\rangle_{vL}$ tabulated in Table III of Ref. [37] are systematically higher than ours. For example, for $5 \leq v \leq 9$ and $L \leq 3$, all 40 of their values are higher than ours, after accounting for the nuclear masses, by up to 3.4×10^{-10}.

TABLE VIII. Nonrelativistic energy $\mathcal{E}^{(2)}$ of Eq. (12), the leading relativistic correction $\mathcal{E}^{(4)}$ of Eq. (22), and the leading QED correction $\mathcal{E}^{(5)}$ of Eq. (25) of the ground electronic state of HD^+ in the Born–Oppenheimer approximation, as functions of the internuclear distance R (atomic units). The last three columns are the contact spin interaction coefficients $\mathcal{A}^{(4)}_{e\gamma}$ and $\mathcal{A}^{(6)}_{e\gamma}$, and $\mathcal{A}^{(7)}_{e\gamma}$ of Eq. (A27). All digits of $\mathcal{E}^{(2)}$, $\mathcal{E}^{(4)}$, $\mathcal{E}^{(5)}$, $\mathcal{A}^{(4)}_{e\gamma}$ and $\mathcal{A}^{(6)}_{e\gamma}$ are are numerically converged to the displayed precision, while the numerical uncertainty of $\mathcal{A}^{(7)}_{e\gamma}$ comes from the small-t extrapolation of $\mathcal{A}^{(7)}_{L'}$, and is given in parentheses when it exceeds one half of the last digit. The last row gives the exact asymptotic values from the analytic formulas.

R	$\mathcal{E}^{(2)}(R)$	$\mathcal{E}^{(4)}(R)$	$\mathcal{E}^{(5)}(R)$	$\mathcal{A}^{(4)}_{e\gamma}(R)$	$\mathcal{A}^{(6)}_{e\gamma}(R)$	$\mathcal{A}^{(7)}_{e\gamma}(R)$
0.1	8.0217579291522481	−1.7689628599497096	113.980903683862	8.4925875070351153	32.282317746656	−2159.331120(7)
0.2	3.0713796982966413	−1.4389128813468541	93.237019490223	6.7090737852806513	17.956254346615	−969.109763(5)
0.3	1.4666292539032291	−1.1531212196195657	76.233151651364	5.3740114727477430	10.758901035474	−513.745819(2)
0.4	0.6992459405698327	−0.9284619818303230	63.056063594903	4.3852492245084879	6.939732097363	−302.348329(1)
0.5	0.2650120000264269	−0.7562294075989127	52.921345203861	3.6457162471019745	4.795335047574	−193.766061(1)
0.6	−0.0048180477784655	−0.6244380044284190	45.071832930313	3.0837513430682842	3.524699675894	−133.843674
0.7	−0.1826248370438247	−0.5229004039104137	38.920414399693	2.6494027212250304	2.733618788643	−98.827418
0.8	−0.3044800944453221	−0.4438780133203365	34.036969643646	2.3081601205559353	2.218566725313	−77.355878
0.9	−0.3902704881246756	−0.3816957789992505	30.110533760544	2.0359966111689939	1.869514983712	−63.628823
1.0	−0.4517863133784512	−0.3322267472399534	26.915685368453	1.8159505224078085	1.624384812110	−54.524635
1.1	−0.4964118670566773	−0.2924614297663106	24.287517317734	1.6358562827073386	1.446752740281	−48.286902
1.2	−0.5289745245003295	−0.2601881550703287	22.103974285603	1.4868465443408775	1.314469939460	−43.888645
1.3	−0.5527406218804872	−0.2337653529383328	20.273582512024	1.3623565544138509	1.213620062930	−40.708726
1.4	−0.5699835280567854	−0.2119614433145061	18.726927930729	1.2574542185093965	1.135192991157	−38.359933
1.5	−0.5823232054549776	−0.1938423480866308	17.410698323658	1.1683828059257004	1.073191740607	−36.594171
1.6	−0.5909372245053716	−0.1786920546438762	16.283477050703	1.0922441089714867	1.023521617378	−35.248436
1.7	−0.5966962695398744	−0.1659560662689392	15.312740050373	1.0267756502067330	0.983319814860	−34.213096
1.8	−0.6002536341023100	−0.1552007632178995	14.472686849069	0.9701917719408994	0.950540204424	−33.412785
1.85	−0.6013667165915524	−0.1504559829600277	14.095043429824	0.9447749634586318	0.936450722377	−33.083578
1.9	−0.6021057828832493	−0.1460839038314011	13.742655717942	0.9210687416741430	0.923689939413	−32.794592
1.95	−0.6025152395971052	−0.1420524803242756	13.413552079363	0.8989379084225687	0.912129750559	−32.541506
2.0	−0.6026342144949465	−0.1383329938679796	13.105952528641	0.8782606089882357	0.901658603344	−32.320623
2.05	−0.6024972590579457	−0.1348996563190293	12.818246910199	0.8589267856585478	0.892178936591	−32.128767
2.1	−0.6021349458445536	−0.1317292660982801	12.548975886334	0.8408368343788357	0.883605063585	−31.963196
2.15	−0.6015743781925450	−0.1288009092983850	12.296814331017	0.8239004347982448	0.875861414794	−31.821530
2.2	−0.6008396265944108	−0.1260956992953139	12.060556791007	0.8080355287572398	0.868881072814	−31.701696
2.3	−0.5989308861578464	−0.1212879739615258	11.631455297939	0.7792280207840891	0.856978736926	−31.520469
2.4	−0.5965536385920330	−0.1171875835531707	11.253973258434	0.7538917377506212	0.847493772064	−31.407396
2.5	−0.5938235109904680	−0.1136965424839047	10.921653732101	0.7315892533648567	0.840099390392	−31.352902
2.6	−0.5908331963248127	−0.1107332876240208	10.629045721392	0.7119519565253180	0.834527459779	−31.349271
2.7	−0.5876572896786272	−0.1082294795765374	10.371518580138	0.6946672159694138	0.830554720518	−31.390150
2.8	−0.5843560034674206	−0.1061274879451224	10.145114520878	0.6794682137502226	0.827992571577	−31.470204
2.9	−0.5809780452697365	−0.1043784007381149	9.946430583729	0.6661258338655831	0.826679413914	−31.584857
3.0	−0.5775628640489736	−0.1029404385386336	9.772523568272	0.6544421466411239	0.826474852295	−31.730102
3.1	−0.5741424157159233	−0.1017776836220909	9.620833000562	0.6442451420810367	0.827255267496	−31.902365
3.2	−0.5707425598956967	−0.1008590559447627	9.489118370492	0.6353844483363284	0.828910413518	−32.098404
3.35	−0.5657259108970165	−0.0998805617232138	9.324750580732	0.6243139746099997	0.832818031494	−32.430554
3.5	−0.5608555387980381	−0.0993133440772031	9.195207448566	0.6155718791311381	0.838171305740	−32.800214
3.75	−0.5531617014029679	−0.0991103106804599	9.043871774825	0.6053181015397773	0.849591954672	−33.476629
4.0	−0.5460848837129383	−0.0996305963763857	8.957779479717	0.5994258055752282	0.863209692453	−34.197227
4.25	−0.5396743135638569	−0.1006837459936110	8.922389033618	0.5969239264892539	0.878089482493	−34.929266
4.5	−0.5339400311092339	−0.1021158201360817	8.925856861495	0.5970222359432166	0.893428753193	−35.643926
4.75	−0.5288662614029215	−0.1037999405796949	8.958356912716	0.5990654979919224	0.908556633143	−36.317036
5.0	−0.5244202951676077	−0.1056309143413121	9.011669401519	0.6025057690017345	0.922939882728	−36.929863
5.5	−0.5172315078578577	−0.1094044936716679	9.154507909045	0.6118293345439856	0.948045688895	−37.929491
6.0	−0.5119690484666523	−0.1129409477807139	9.313388965963	0.6222602355398188	0.967204368357	−38.608906
7.0	−0.5055940042392590	−0.1184130822016879	9.592044680022	0.6406161836030249	0.989178837117	−39.190958
8.0	−0.5025703885999690	−0.1216660854064982	9.775367253696	0.6527177338096528	0.997345149253	−39.215695
9.0	−0.5011954528983677	−0.1233668234219922	9.878168978140	0.6595116290844090	0.999703634642	−39.087594
10.0	−0.5005787289439264	−0.1241981389540587	9.931301955458	0.6630259155785928	1.000161993028	−38.965701
11.0	−0.5002992293703975	−0.1245932668988955	9.957738695680	0.6647757399967498	1.000138659097	−38.883432
12.0	−0.5001683069678789	−0.1247811608623925	9.970769026369	0.6656388316787986	1.000051483682	−38.834821
∞	−0.5	−0.125	9.98625612749328	0.6666666666666667	1	−38.774038755

TABLE IX. The rovibrational averages δ and Δ defined in Eqs. (43)–(46). $\delta^{(6)}_{vL}$ is converged to all digits shown. The uncertainties of $\Delta^{(6)}_{vL}$ and $\delta^{(7)}_{vL}$ ($\sim 10^{-9}$) come from the interpolation of $\mathcal{A}^{(6)}_{e\gamma}(R)$ and $\mathcal{E}^{(5)}(R)$ between the grid points of Table VIII, and that of $\Delta^{(7)}_{vL}$ ($\sim 10^{-6}$) from the numerical uncertainty of $\mathcal{A}^{(7)}_{e\gamma}(R)$.

v	L	$\delta^{(6)}_{vL}$	$\Delta^{(6)}_{vL}$	$\Delta^{(6)}_{vL}+\delta^{(6)}_{vL}$	$\delta^{(7)}_{vL}$	$\Delta^{(7)}_{vL}$	$\Delta^{(7)}_{vL}+\delta^{(7)}_{vL}$
0	0	0.2681776981	−0.4033505589	−0.1351728608	−22.2530170	18.169944	−4.083073
0	1	0.2671480044	−0.4025706898	−0.1354226855	−22.1795966	18.132692	−4.046905
0	2	0.2651052188	−0.4010177984	−0.1359125796	−22.0338726	18.058515	−3.975358
0	3	0.2620818686	−0.3987053921	−0.1366235235	−21.8180347	17.948060	−3.869975
1	0	0.2463125331	−0.3772818356	−0.1309693026	−20.5906329	16.927683	−3.662950
1	1	0.2453427822	−0.3765367795	−0.1311939973	−20.5213351	16.892111	−3.629225
1	2	0.2434189934	−0.3750530921	−0.1316340987	−20.3837971	16.821272	−3.562525
1	3	0.2405719423	−0.3728434482	−0.1322715059	−20.1800911	16.715774	−3.464317
2	0	0.2255520032	−0.3521027919	−0.1265507887	−19.0111183	15.727750	−3.283368
2	1	0.2246378134	−0.3513894153	−0.1267516019	−18.9456258	15.693705	−3.251921
2	2	0.2228243183	−0.3499687005	−0.1271443822	−18.8156428	15.625903	−3.189740
2	3	0.2201406622	−0.3478525601	−0.1277118979	−18.6231324	15.524912	−3.098220
3	0	0.2057782457	−0.3277134807	−0.1219352350	−17.5054210	14.565422	−2.939999
3	1	0.2049157769	−0.3270289634	−0.1221131865	−17.4434512	14.532769	−2.910683
3	2	0.2032049512	−0.3256656139	−0.1224606627	−17.3204618	14.467732	−2.852729
3	3	0.2006733920	−0.3236346472	−0.1229612552	−17.1383136	14.370847	−2.767466
4	0	0.1868910692	−0.3040263301	−0.1171352609	−16.0656393	13.436612	−2.629027
4	1	0.1860769921	−0.3033681529	−0.1172911608	−16.0069419	13.405229	−2.601713
4	2	0.1844622285	−0.3020571608	−0.1175949323	−15.8904488	13.342719	−2.547730
4	3	0.1820729839	−0.3001039320	−0.1180309481	−15.7179254	13.249584	−2.468342
5	0	0.1688073814	−0.2809661862	−0.1121588048	−14.6849627	12.337882	−2.347080
5	1	0.1680388585	−0.2803321264	−0.1122932679	−14.6293180	12.307665	−2.321653
5	2	0.1665145304	−0.2790690750	−0.1125545447	−14.5188849	12.247471	−2.271414
5	3	0.1642592808	−0.2771870303	−0.1129277495	−14.3553394	12.157776	−2.197563
6	0	0.1514611075	−0.2584707157	−0.1070096082	−13.3576445	11.266479	−2.091165
6	1	0.1507357865	−0.2578588504	−0.1071230638	−13.3048623	11.237338	−2.067524
6	2	0.1492972356	−0.2566399215	−0.1073426858	−13.2001117	11.179284	−2.020828
6	3	0.1471691082	−0.2548234014	−0.1076542932	−13.0449851	11.092767	−1.952218
7	0	0.1348035840	−0.2364911722	−0.1016875882	−12.0790044	10.220388	−1.858616
7	1	0.1341196040	−0.2358998902	−0.1017802862	−12.0289237	10.192251	−1.836673
7	2	0.1327631526	−0.2347218877	−0.1019587352	−11.9295364	10.136193	−1.793344
7	3	0.1307567414	−0.2329661643	−0.1022094228	−11.7823569	10.052642	−1.729715
8	0	0.1188044132	−0.2149935282	−0.0961891150	−10.8454612	9.198411	−1.647050
8	1	0.1181604223	−0.2144215496	−0.0962611273	−10.7979508	9.171224	−1.626727
8	2	0.1168834104	−0.2132819402	−0.0963985298	−10.7036669	9.117056	−1.586611
8	3	0.1149948348	−0.2115832778	−0.0965884430	−10.5640513	9.036315	−1.527737
9	0	0.1034527565	−0.1939599604	−0.0905072039	−9.6545963	8.200272	−1.454324
9	1	0.1028479428	−0.1934063652	−0.0905584224	−9.6095559	8.174002	−1.435554
9	2	0.1016487908	−0.1923033347	−0.0906545439	−9.5201774	8.121658	−1.398519
9	3	0.0998757911	−0.1906590766	−0.0907832855	−9.3878351	8.043633	−1.344202

TABLE X. The electron–proton coupling $A_{ep} = \bar{A}_{ep} + A_{ep}^{(6)} + A_{ep}^{(7)}$ of Eq. (42) and its three parts (in Hz): $A_{ep}^{(6)}$, $A_{ep}^{(7)}$, and $\bar{A}_{ep} = \langle \pi\delta^{(3)}(r_{ep})\rangle_{vL}\,(1+m/m_p)^3\,A_p^{\rm exp}$, with the nonadiabatic (three-body) expectation values $\langle \pi\delta^{(3)}(r_{ep})\rangle_{vL}$ of the first data column recalculated here with the CODATA 2022 mass ratios from Table VI. The numerical uncertainty of $A_{ep}^{(6)}$ is $\sim 5\cdot 10^{-5}$ Hz, that of $A_{ep}^{(7)}$ is $\sim 2\cdot 10^{-4}$ Hz, and that of $\bar{A}_{ep}$ is ~ 0.01 Hz (the 12 digits of $\langle \pi\delta^{(3)}\rangle_{vL}$ and the experimental value). The total uncertainty of A_{ep} (shown in Table I) is dominated by the unknown higher-order terms of Eq. (42).

v	L	$\langle \pi\delta^{(3)}(r_{ep})\rangle_{vL}$	$\bar{A}_{ep}$ (Hz)	$A_{ep}^{(6)}$ (Hz)	$A_{ep}^{(7)}$ (Hz)	A_{ep} (Hz)
0	0	0.650443509501	925404029.05	−7672.27671	−538.3160	925395818.46
0	1	0.649862629319	924577594.70	−7686.45651	−533.5476	924569374.70
0	2	0.648707155951	922933670.68	−7714.26241	−524.1148	922925432.30
0	3	0.646989479822	920489885.19	−7754.61488	−510.2210	920481620.35
1	0	0.635509211376	904156588.72	−7433.68694	−482.9266	904148672.11
1	1	0.634960524247	903375956.32	−7446.44039	−478.4803	903368031.40
1	2	0.633869164175	901823248.06	−7471.42011	−469.6865	901815306.96
1	3	0.632246981701	899515324.05	−7507.59870	−456.7387	899507359.71
2	0	0.621551029546	884297896.13	−7182.89651	−432.8822	884290280.35
2	1	0.621033039067	883560936.70	−7194.29446	−428.7362	883553313.67
2	2	0.620002813886	882095206.75	−7216.58828	−420.5382	882087569.63
2	3	0.618471693396	879916839.15	−7248.79990	−408.4721	879909181.88
3	0	0.608513974390	865749716.02	−6920.92228	−387.6121	865742407.48
3	1	0.608025345054	865054529.50	−6931.02263	−383.7470	865047214.73
3	2	0.607053597129	863671996.77	−6950.74503	−376.1065	863664669.92
3	3	0.605609585591	861617561.48	−6979.15816	−364.8653	861610217.46
4	0	0.596348750375	848441914.26	−6648.48054	−346.6134	848434919.16
4	1	0.595888295787	847786812.74	−6657.32926	−343.0122	847779812.40
4	2	0.594972664819	846484119.16	−6674.57103	−335.8951	846477108.69
4	3	0.593612252966	844548623.46	−6699.31885	−325.4284	844541598.72
5	0	0.585011187222	832311648.57	−6366.02186	−309.4412	832304973.11
5	1	0.584577859909	831695141.78	−6373.65385	−306.0888	831688462.04
5	2	0.583716262653	830469323.46	−6388.48366	−299.4652	830462635.51
5	3	0.582436354837	828648363.09	−6409.66639	−289.7287	828641663.70
6	0	0.574461716426	817302623.75	−6073.75859	−275.7011	817296274.29
6	1	0.574054598849	816723406.28	−6080.19822	−272.5843	816717053.50
6	2	0.573245211232	815571868.06	−6092.66375	−266.4278	815565508.97
6	3	0.572043098825	813861589.38	−6110.35027	−257.3822	813855221.65
7	0	0.564664866368	803364373.34	−5771.68605	−245.0417	803358356.61
7	1	0.564283162614	802821312.82	−5776.94749	−242.1486	802815293.72
7	2	0.563524403186	801741804.72	−5787.07608	−236.4361	801735781.21
7	3	0.562397739942	800138869.67	−5801.30486	−228.0472	800132840.31
8	0	0.555588737742	790451513.30	−5459.59820	−217.1486	790445836.56
8	1	0.555231765090	789943638.41	−5463.68555	−214.4692	789937960.25
8	2	0.554522278195	788934231.71	−5471.48437	−209.1803	788928551.05
8	3	0.553469055070	787435781.95	−5482.26365	−201.4182	787430098.27
9	0	0.547204397912	778522880.38	−5137.09859	−191.7394	778517551.55
9	1	0.546871576857	778049366.63	−5140.00571	−189.2648	778044037.36
9	2	0.546210212619	777108425.38	−5145.46146	−184.3821	777103095.54
9	3	0.545228727647	775712039.48	−5152.76871	−177.2209	775706709.49

TABLE XI. The electron–deuteron coupling $A_{ed} = \bar{A}_{ed} + A_{ed}^{(6)} + A_{ed}^{(7)}$ of Eq. (42) and its three parts (in Hz): $A_{ed}^{(6)}$, $A_{ed}^{(7)}$, and $\bar{A}_{ed} = \langle\pi\delta^{(3)}(r_{ed})\rangle_{vL}\,(1+m/m_d)^3\,A_d^{\rm exp}$, with the nonadiabatic (three-body) expectation values $\langle\pi\delta^{(3)}(r_{ed})\rangle_{vL}$ of the first data column recalculated here with the CODATA 2022 mass ratios from Table VI. The numerical uncertainty of $A_{ed}^{(6)}$ is $\sim 10^{-5}$ Hz, that of $A_{ed}^{(7)}$ is $\sim 3\cdot 10^{-5}$ Hz, and that of $\bar{A}_{ed}$ is ~ 0.01 Hz (the 12 digits of $\langle\pi\delta^{(3)}\rangle_{vL}$ and the experimental value). The total uncertainty of A_{ed} (shown in Table I) is dominated by the unknown higher-order terms of Eq. (42).

v	L	$\langle\pi\delta^{(3)}(r_{ed})\rangle_{vL}$	$\bar{A}_{ed}$ (Hz)	$A_{ed}^{(6)}$ (Hz)	$A_{ed}^{(7)}$ (Hz)	A_{ed} (Hz)
0	0	0.651403398955	142289087.29	−1177.74131	−82.6348	142287826.92
0	1	0.650822518150	142162202.78	−1179.91800	−81.9028	142160940.96
0	2	0.649667048722	141909808.20	−1184.18637	−80.4548	141908543.56
0	3	0.647949391364	141534612.28	−1190.38072	−78.3220	141533343.58
1	0	0.636490374341	139031565.66	−1141.11632	−74.1322	139030350.42
1	1	0.635941784883	138911734.71	−1143.07406	−73.4496	138910518.18
1	2	0.634850625540	138673387.67	−1146.90860	−72.0998	138672168.67
1	3	0.633228757533	138319115.47	−1152.46223	−70.1122	138317892.89
2	0	0.622559347762	135988546.45	−1102.61846	−66.4501	135987377.38
2	1	0.622041569564	135875445.74	−1104.36812	−65.8136	135874275.56
2	2	0.621011774696	135650502.84	−1107.79036	−64.5552	135649330.49
2	3	0.619481313982	135316197.16	−1112.73504	−62.7030	135315021.72
3	0	0.609556441086	133148260.81	−1062.40382	−59.5008	133147138.90
3	1	0.609068160321	133041603.36	−1063.95428	−58.9075	133040480.50
3	2	0.608097115890	132829493.59	−1066.98179	−57.7346	132828368.87
3	3	0.606654175408	132514305.36	−1071.34338	−56.0090	132513178.01
4	0	0.597433818898	130500259.82	−1020.58235	−53.2073	130499186.03
4	1	0.596973878228	130399792.83	−1021.94068	−52.6545	130398718.23
4	2	0.596059282375	130200013.38	−1024.58740	−51.5619	130198937.23
4	3	0.594700441367	129903195.39	−1028.38634	−49.9553	129902117.05
5	0	0.586149251644	128035319.08	−977.22322	−47.5011	128034294.35
5	1	0.585716642996	127940822.35	−978.39477	−46.9865	127939796.97
5	2	0.584856491769	127752935.50	−980.67124	−45.9697	127751908.86
5	3	0.583578774760	127473837.80	−983.92292	−44.4751	127472809.41
6	0	0.575665787676	125745367.07	−932.35902	−42.3218	125744392.39
6	1	0.575259647743	125656652.03	−933.34754	−41.8433	125655676.84
6	2	0.574452226273	125480283.19	−935.26108	−40.8983	125479307.03
6	3	0.573253090307	125218350.32	−937.97607	−39.5097	125217372.83
7	0	0.565951544832	123623439.63	−885.98904	−37.6154	123622516.03
7	1	0.565571153722	123540349.02	−886.79671	−37.1713	123539425.06
7	2	0.564815033739	123375186.20	−888.35151	−36.2944	123374261.56
7	3	0.563692365217	123129956.47	−890.53571	−35.0066	123129030.93
8	0	0.556979647512	121663666.19	−838.08165	−33.3336	121662794.77
8	1	0.556624431394	121586074.67	−838.70908	−32.9223	121585203.04
8	2	0.555918476824	121431869.72	−839.90625	−32.1105	121430997.70
8	3	0.554870600663	121202977.23	−841.56094	−30.9189	121202104.75
9	0	0.548728361954	119861299.34	−788.57599	−29.4332	119860481.33
9	1	0.548397901339	119789115.29	−789.02225	−29.0533	119788297.21
9	2	0.547741285305	119645687.58	−789.85975	−28.3038	119644869.41
9	3	0.546766991555	119432868.04	−790.98145	−27.2045	119432049.86